Mutational, Kinetic, and NMR Studies of the Roles of Conserved Glutamate Residues and of Lysine-39 in the Mechanism of the MutT Pyrophosphohydrolase†

Thomas K. Harris,‡ Gong Wu,‡ Michael A. Massiah, and Albert S. Mildvan*

Department of Biological Chemistry, The Johns Hopkins School of Medicine, 725 North Wolfe Street, Baltimore, Maryland 21205-2185

Received August 11, 1999; Revised Manuscript Received October 28, 1999

ABSTRACT: The MutT enzyme catalyzes the hydrolysis of nucleoside triphosphates (NTP) to NMP and PP_i by nucleophilic substitution at the rarely attacked β-phosphorus. The solution structure of the quaternary $E-M^{2+}-AMPCPP-M^{2+}$ complex indicated that conserved residues Glu-53, -56, -57, and -98 are at the active site near the bound divalent cation possibly serving as metal ligands, Lys-39 is positioned to promote departure of the NMP leaving group, and Glu-44 precedes helix I (residues 47−59) possibly stabilizing this helix which contributes four catalytic residues to the active site [Lin, J., Abeygunawardana, C., Frick, D. N., Bessman, M. J., and Mildvan, A. S. (1997) *Biochemistry 36*, 1199−1211]. To test these proposed roles, the effects of mutations of each of these residues on the kinetic parameters and on the Mn^{2+}, Mg^{2+}, and substrate binding properties were examined. The largest decreases in k_{cat} for the Mg^{2+}-activated enzyme of $10^{4.7}$- and $10^{2.6}$-fold were observed for the E53Q and E53D mutants, respectively, while 97-, 48-, 25-, and 14-fold decreases were observed for the E44D, E56D, E56Q, and E44Q mutations, respectively. Smaller effects on k_{cat} were observed for mutations of Glu-98 and Lys-39. For wild type MutT and its E53D and E44D mutants, plots of $\log(k_{cat})$ versus pH exhibited a limiting slope of 1 on the ascending limb and then a hump, i.e., a sharply defined maximum near pH 8 followed by a plateau, yielding apparent pK_a values of 7.6 ± 0.3 and 8.4 ± 0.4 for an *essential* base and a *nonessential* acid catalyst, respectively, in the active quaternary $MutT-Mg^{2+}-dGTP-Mg^{2+}$ complex. The pK_a of 7.6 is assigned to Glu-53, functioning as a base catalyst in the active quaternary complex, on the basis of the disappearance of the ascending limb of the pH−rate profile of the E53Q mutant, and its restoration in the E53D mutant with a $10^{1.9}$-fold increase in $(k_{cat})^{max}$. The pK_a of 8.4 is assigned to Lys-39 on the basis of the disappearance of the descending limb of the pH−rate profile of the K39Q mutant, and the observation that removal of the positive charge of Lys-39, by either deprotonation or mutation, results in the same 8.7-fold decrease in k_{cat}. Values of k_{cat} of both wild type MutT and the E53Q mutant were independent of solvent viscosity, indicating that a chemical step is likely to be rate-limiting with both. A liganding role for Glu-53 and Glu-56, but not Glu-98, in the binary $E-M^{2+}$ complex is indicated by the observation that the E53Q, E53D, E56Q, and E56D mutants bound Mn^{2+} at the active site 36-, 27-, 4.7-, and 1.9-fold weaker, and exhibited 2.10-, 1.50-, 1.12-, and 1.24-fold lower enhanced paramagnetic effects of Mn^{2+}, respectively, than the wild type enzyme as detected by $1/T_1$ values of water protons, consistent with the loss of a metal ligand. However, the K_m values of Mg^{2+} and Mn^{2+} indicate that Glu-56, and to a lesser degree Glu-98, contribute to metal binding in the active quaternary complex. Mutations of the more distant but conserved residue Glu-44 had little effect on metal binding or enhancement factors in the binary $E-M^{2+}$ complexes. Two-dimensional $^1H-^{15}N$ HSQC and three-dimensional $^1H-^{15}N$ NOESY-HSQC spectra of the kinetically damaged E53Q and E56Q mutants showed largely intact proteins with structural changes near the mutated residues. Structural changes in the kinetically more damaged E44D mutant detected in $^1H-^{15}N$ HSQC spectra were largely limited to the loop I−helix I motif, suggesting that Glu-44 stabilizes the active site region. $^1H-^{15}N$ HSQC titrations of the E53Q, E56Q, and E44D mutants with dGTP showed changes in chemical shifts of residues lining the active site cleft, and revealed tighter nucleotide binding by these mutants, indicating an intact substrate binding site. A mechanism is proposed in which Glu-53 coordinates the metal in the binary $MutT-M^{2+}$ complex, dissociates from the metal and orients and deprotonates the attacking water ligand in the quaternary $MutT-M^{2+}-dGTP-M^{2+}$ complex, and subsequently facilitates the displacement of PP_i-M^{2+} from the $MutT-M^{2+}-PP_i-M^{2+}$ product complex. From the effects of single mutations on k_{cat}, the 10^9-fold rate acceleration produced by wild type MutT can now be explained quantitatively by the cooperative effects of the enzyme- and nucleotide-bound divalent cations, with Glu-53 activating the attacking water nucleophile, and Lys-39 promoting the departure of the dGMP leaving group.

The MutT enzyme, a pyrophosphohydrolase of 129 residues from *Escherichia coli*, catalyzes the unusual hydrolysis of nucleoside and deoxynucleoside triphosphates (NTP)[1] by nucleophilic substitution at the rarely attacked β-phosphorus, yielding inorganic pyrophosphate (PP_i) and a nucleotide (NMP) (*1*, *2*):

$$NTP^{4-} + H_2O \xrightarrow[2M^{2+}]{MutT} NMP^{2-} + PP_i^{4-} + 2H^+ \quad (1)$$

The MutT enzyme accelerates this reaction by a factor of

10.1021/bi9918745 CCC: $19.00
Published on Web 01/29/2000

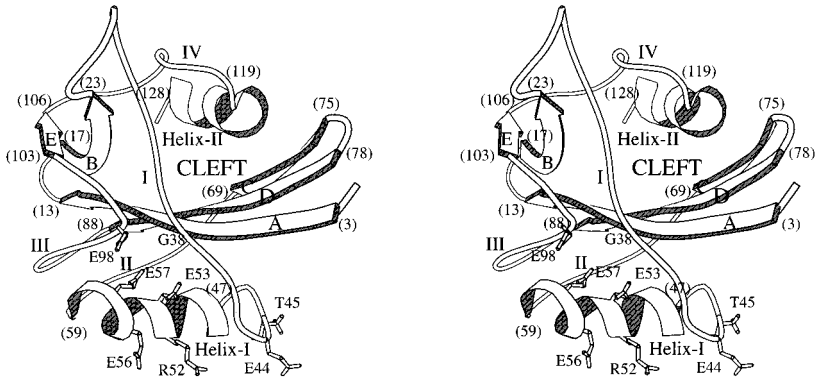

FIGURE 1: Stereoview of the solution structure of the free MutT enzyme with the lowest van der Waals energy (*11*) in which the secondary structural elements, the nucleotide binding cleft, and conserved residues are labeled. The numbers in parentheses denote residues at the beginnings and ends of the secondary structural components.

$10^{9.0}$, a catalytic power typical for enzymes which catalyze nucleophilic substitution at the electron-rich β-phosphorus of NTP with pyrophosphoryl transfer (*3*).

The biological role of the MutT enzyme is to prevent AT → CG transversions (*4*) by preferentially hydrolyzing a mutagenic form of dGTP which mispairs with template adenine during DNA replication, thus "sanitizing" the nucleotide pool (*1*, and references therein). Maki and Sekiguchi (*5*) have proposed that the biological substrate of the MutT enzyme is 8-oxo-dGTP, an oxidatively modified nucleotide which readily mispairs with template adenine during DNA synthesis in vitro (*6*), and Sekiguchi and coworkers have characterized similar enzymes from a human cell line (*7*, *8*) and from mice (*9*).

Like the seven other enzymes which are currently known to catalyze nucleophilic substitution at the electron-rich β-phosphorus of NTP, most of which are synthetases, MutT requires two divalent cations for activity, one coordinated by the NTP and the other coordinated by the enzyme (*10*). MutT was the first enzyme in this small class of pyrophosphotransferases to have its tertiary structure determined (*11*). This solution structure found the conserved residues among the MutT-related hydrolases to be located along the loop I−helix I and loop III regions of this α/β-protein (Figure 1).

The solution structure of the quaternary MutT−M^{2+}−AMPCPP−M^{2+} complex, which mimics the active complex, showed that the enzyme-bound divalent cation coordinates two water ligands and binds near the side chain carboxylate groups of Glu-56, -57, and -98, and the backbone carbonyl group of Gly-38, as found by paramagnetic broadening by Mn^{2+} and Co^{2+} of their $CH_2-{}^{13}CO_2^-$ cross-peaks in two-dimensional CO(C)H spectra, suggesting that they function as metal ligands (Figure 2) (*12*). $Co^{3+}(NH_3)_4$AMPCPP, a nonhydrolyzable analogue of the substrate ATP−Mg^{2+}, was found to bind in the second coordination sphere of the enzyme-bound divalent cation with an intervening water ligand of the metal ion (w2, Figure 2) approaching the β-phosphorus of AMPCPP, in position to attack it. Lys-39 approached the α-phosphate of the NMP leaving group, presumably positioned to promote its departure. The role of Glu-53 in catalysis could not be determined because its δ-${}^{13}COO^-$ resonance was not detected by NMR (*12*). However, in the computed structures of the quaternary complex, Glu-53 is well positioned to accept a hydrogen bond from the metal-bound water (w2) at a distance of 2.6 $\pm$ 0.2 Å, suggesting a role for this residue either as a general base or in orienting the attacking water or hydroxyl ligand of the enzyme-bound metal (Figure 2). The orientation of the side chain of the conserved residue Arg-52, though not well defined in the structure, was too far from the triphosphate of bound AMPCPP to interact with it. One of the $N\eta H_2$ groups of Arg-52 could, by rotation of the side chain, approach a carboxylate oxygen of Glu-53 to within hydrogen-bonding distance, suggesting that Arg-52 may orient Glu-53 which in turn may orient and deprotonate the attacking water.

Previous mutagenesis studies support the proposed roles of Glu-57 (*13*), Lys-39 (*14*), and Arg-52 (*12*, *14*). In support of an important liganding role for Glu-57, the catalytic activity of the E57Q mutant was at least 10^5-fold lower than that of the wild type enzyme, but the global fold of the protein was preserved on the basis of comparisons of $^1H-{}^{15}N$ NOESY-HSQC spectra and $^1H-{}^{15}N$ HSQC spectra to those of the wild type enzyme (*13*). The affinity of the enzyme for both Mg^{2+} and Mn^{2+} decreased 3.3−3.6-fold, while the affinity for dGTP was essentially unaltered, suggesting that Glu-57 is one of the ligands to the enzyme-bound divalent cation. The K39Q mutation decreased k_{cat} 8-fold, and the R52Q mutation decreased k_{cat} at least 10^3-fold (*12*, *14*).

Since the only way that Arg-52 can function in catalysis is by orienting Glu-53, it was necessary to mutate Glu-53 to directly determine its role in catalysis. Mutations of Glu-53 to Gln and Asp are shown here to have profound effects on catalysis and minimal effects on enzyme structure, defining

† This research was supported by National Institutes of Health Grant DK28616 to A.S.M.

* To whom correspondence should be addressed. Phone: (410) 955-2038. Fax: (410) 955-5759. E-mail: mildvan@welchlink.welch.jhu.edu.

‡ These authors contributed equally to this work.

[1] Abbreviations: AMPCPP, α,β-methyleneadenosine 5′-triphosphate; EDTA, (ethylenedinitrilo)tetraacetic acid; EPR, electron paramagnetic resonance; HSQC, heteronuclear single-quantum coherence; IPTG, isopropyl β-D-thiogalactoside; LB/Amp, Luria-Bertani medium containing ampicillin; NMP, nucleoside monophosphates; NMR, nuclear magnetic resonance; NOESY, nuclear Overhauser effect spectroscopy; NTP, nucleoside triphosphates; PCR, polymerase chain reaction; PEI, polyethyleneimine cellulose; PP_i, inorganic pyrophosphate; SDS−PAGE, sodium dodecyl sulfate−polyacrylamide gel electrophoresis; TLC, thin-layer chromatography; TOCSY, total correlation spectroscopy; TPPI, time-proportional phase incrementation; TSP, sodium 3-(trimethylsilyl)propionate-2,2,3,3-d_4.

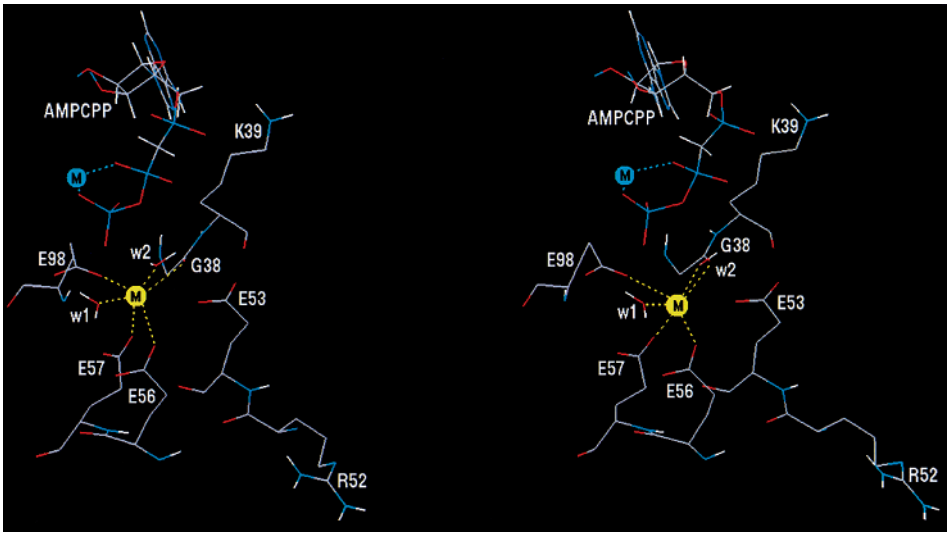

FIGURE 2: Stereoview of the active site region of the solution structure of the quaternary MutT−M^{2+}−AMPCPP−M^{2+} complex (*12*) showing likely metal ligands (G38, E56, E57, and E98) and catalytic residues (K39 and E53). The water ligand (w2), cis to Gly-38 and near both the β-phosphorus and Glu-53, is well positioned to be the attacking nucleophile.

more clearly the role and contribution of Glu-53 to catalysis. In addition, two proposed ligands of the enzyme-bound divalent cation, Glu-56 and Glu-98, located in helix I, and a conserved residue Glu-44, located in loop I which precedes and may stabilize helix I (residues 47−59, Figure 1), were mutated to both Gln and Asp. The kinetic, metal binding, and substrate binding properties of these mutants were investigated as well as the structures of the catalytically damaged E53Q, E56Q, and E44D mutants. Preliminary abstracts of this work have been published (*15*, *16*).

EXPERIMENTAL PROCEDURES

Materials. The construction of the plasmid pETMutT which contains the gene for MutT under control of the T7 expression system (pET system; Novagen, Inc., Madison, WI) has been described previously (*17*). The DNA-mismatched primers for site-directed mutagenesis were synthesized by Operon Technologies, Inc. (Alameda, CA). The expression vector pET11b, the T7 promoter primer, and the T7 terminator primer were from Novagen, Inc. The Expand High Fidelity PCR System enzyme mix and buffer, the DNA polymerization mix, restriction enzymes, T4 ligase, and isopropyl β-D-thiogalactoside (IPTG) were from Boehringer Mannheim (Indianapolis, IN). Thin-walled PCR tubes were from Ambion, Inc. (Austin, TX). Tryptone and yeast extract were obtained from Difco (Detroit, MI). Centricon (10 000 MW cutoff) centrifugal microconcentrators were from Amicon (Beverly, MA). The Wizard Plus Miniprep and Midiprep DNA Purification Systems were from Promega Corp. (Madison, WI). The QIAquick PCR Purification Kit and QIAEXII Gel Extraction Kit were from QIAGEN (Valencia, CA). Sephadex G-100 and DEAE-Sepharose fast-flow were from Pharmacia Biotech (Piscataway, NJ). Deuterium oxide (D_2O, 99.96% D) was from Aldrich (Milwaukee, WI). Uniformly ^{15}N-enriched $^{15}NH_4Cl$ (99%) and ^{13}C-enriched D-[$^{13}C_6$]glucose (99%) were from Cambridge Isotope Labs, Inc. (Andover, MA). [γ-^{32}P]ATP (4×10^6 Ci/mol) and EcoLite (+) scintillation cocktail were from ICN Biomedicals, Inc. (Costa Mesa, CA). All solvents and reagents were of the highest purity grade available, and buffers were treated with Chelex-100 before use to remove trace metals.

Strains. E. coli strain DH5α was from Life Technologies GibcoBRL (Gaithersburg, MD) and was used for transformation of ligated plasmids. *E. coli* strain HMS174 (DE3) was from Novagen, Inc., and was used for expression of the recombinant proteins. This strain, which overexpressed the K39Q mutant of MutT, was generously provided by M. Bessman. Cells for general cloning and expression were grown in LB medium (*18*) supplemented with ampicillin (100 μg/mL).

General Methods. Techniques for restriction enzyme digestions, ligation, transformation, and other standard molecular biology manipulations have been described (*18*). Plasmid DNA was prepared using the Wizard Plus Miniprep and Midiprep DNA Purification Systems from Promega which provides the reagents for the extraction of DNA from bacterial cells by the alkaline lysis method. DNA sequencing was carried out at the Biosynthesis and Sequencing Facility in the Department of Biological Chemistry at Johns Hopkins University School of Medicine. The concentration of MutT was determined spectrophotometrically using an $A_{280}^{1mg/mL}$ of 2.2 (*10*). Concentrations of dGTP were determined using an ϵ_{252} of 1.37×10^4 M^{-1} cm^{-1} (*10*). Ultraviolet−visible spectroscopy was performed on a Beckman DU640 spectrophotometer. The solution pH was measured with a Beckman Φ10 pH meter and an Aldrich combination electrode, calibrated with Fisher standard buffer solutions. Samples (60 μL) for radiochemical analysis were dissolved in scintillation cocktail (7 mL) and counted in a Beckman LS 6000SE automatic liquid scintillation counter. Linear and nonlinear regression analyses of kinetic and binding data were performed using the Grafit program (Erithacus Software Ltd., Staines, U.K.).

Preparation of the Gln and Asp Mutants at Glu-44, -53, -56, and -98 of E. coli MutT. The megaprimer method of Sarkar and Sommer (*19*) as modified by Barik (*20*) was used to prepare the mutants (Table 1). The gene for MutT in the plasmid pETMutT (*17*) was used as the template for a polymerase chain reaction (PCR) with the following prim-

Table 1: Kinetic Parameters for Mg^{2+} and Mn^{2+} Activation of the dGTPase of the Conserved Glutamate Mutants of MutT Compared to Those of the Wild Type Enzyme[a]

enzyme	$K_a^{Mg^{2+}}$ (mM)	$K_m^{Mg^{2+}}$ (mM)	$K_s^{dGTP-Mg^{2+}}$ (mM)	$K_m^{dGTP-Mg^{2+}}$ (mM)	k_{cat} (s^{-1})	fold decrease in k_{cat}
			Mg^{2+} Activation			
wild type[c]	15 ± 7	1.7 ± 0.7	13 ± 6	0.28 ± 0.8	(4.0 ± 0.1), 10^{b}	1
E44Q	25 ± 2	10 ± 1	3.8 ± 0.2	1.2 ± 0.1	$(2.9 \pm 0.1) \times 10^{-1}$	14
E44D	13 ± 1	7.7 ± 0.1	1.7 ± 0.1	0.75 ± 0.07	$(4.1 \pm 0.2) \times 10^{-2}$	$10^{2.0}$
E53Q					$(1.8 \pm 0.2) \times 10^{-4}$	$(10^{4.7})^{b}$
E53D	36 ± 6	5.0 ± 1.0	1.0 ± 0.3	0.14 ± 0.02	$(1.0 \pm 0.1) \times 10^{-2}$	$10^{2.6}$
E56Q	32 ± 4	8.8 ± 0.2	1.1 ± 0.1	0.24 ± 0.01	$(1.6 \pm 0.1) \times 10^{-1}$	$10^{1.4}$
E56D	16 ± 1	4.9 ± 0.2	1.7 ± 0.1	1.2 ± 0.2	$(8.4 \pm 0.8) \times 10^{-2}$	$10^{1.7}$
E98Q	21 ± 1	11 ± 1	0.75 ± 0.02	0.36 ± 0.02	$(6.3 \pm 0.5) \times 10^{-1}$	6.4
E98D	55 ± 1	15 ± 1	1.1 ± 0.1	0.64 ± 0.05	$(7.1 \pm 0.6) \times 10^{-1}$	5.6
enzyme	$K_a^{Mn^{2+}}$ (μM)	$K_m^{Mn^{2+}}$ (μM)	$K_s^{dGTP-Mn^{2+}}$ (μM)	$K_m^{dGTP-Mn^{2+}}$ (μM)	k_{cat} (s^{-1})	fold decrease in k_{cat}
			Mn^{2+} Activation			
wild type[c]	230 ± 70	26 ± 10	22 ± 13	6.3 ± 0.5	$(1.9 \pm 0.1) \times 10^{-1}$, 0.50^{b}	1
E44Q	390 ± 10	360 ± 100	260 ± 10	200 ± 30	$(1.0 \pm 0.2) \times 10^{-1}$	1.9
E44D	840 ± 20	220 ± 10	370 ± 10	110 ± 10	$(2.7 \pm 0.2) \times 10^{-2}$	7.0
E53Q					$(\leq 0.5 \times 10^{-5})^{d}$	$(\geq 10^{5})^{d}$
E53D	3300 ± 600	1500 ± 200	330 ± 100	130 ± 10	$(1.1 \pm 0.1) \times 10^{-3}$	$10^{2.2}$
E56Q	870 ± 10	560 ± 50	76 ± 2	56 ± 3	$(1.3 \pm 0.1) \times 10^{-1}$	1.5
E56D	560 ± 10	200 ± 10	61 ± 2	45 ± 7	$(4.3 \pm 0.2) \times 10^{-2}$	4.4
E98Q	330 ± 10	78 ± 5	40 ± 2	34 ± 3	$(1.1 \pm 0.1) \times 10^{-1}$	1.7
E98D	900 ± 140	320 ± 40	85 ± 4	59 ± 4	$(1.3 \pm 0.1) \times 10^{-1}$	1.5

[a] Conditions were 50 mM Tris-HCl buffer, pH 7.5, and 23 °C. [b] Conditions were 50 mM Tris-HCl buffer, pH 7.5, and 37 °C. [c] From ref *10*. [d] No activity was detected indicating a $\geq 10^5$-fold loss of activity.

ers: E44Q, 5′-TTC CGG CGT TTG ACC CAT TTC-3′; E44D, 5′-TTC CGG CGT ATC ACC CAT TTC-3′; E53Q, 5′-TTC CTG AAG TTG ACG CAC CAC-3′; E53D, 5′-TTC CTG AAG ATC ACG CAC CAC-3′; E56Q, 5′-CCC GAC TTC TTG CTG AAG TTC-3′; E56D, 5′-CCC GAC TTC ATC CTG AAG TTC-3′; E98Q, 5′-GGG TTG CCC TTG TTT ACC CCA-3′; and E98D, 5′-GGG TTG CCC ATC TTT ACC CCA-3′. Each primer is complementary to the coding strand but contains the appropriate mispair (underlined) in the codon designating the amino acid to be mutated. The second primer was upstream of the MutT gene (T7 promoter primer). The resulting DNA product was isolated using the QIAquick PCR Purification Kit and used in a second PCR as a "megaprimer" with a primer downstream of the MutT gene (T7 terminator primer) and the plasmid pETMutT as the template. PCRs were carried out with the Expand High Fidelity PCR System utilizing both Taq DNA polymerase and Pwo DNA polymerase which results in increased fidelity of DNA synthesis due to the inherent 3′−5′ exonuclease proofreading activity of Pwo DNA polymerase (*21*). The reaction protocol consisted of 35 cycles, a 5 min incubation period at 94 °C preceding the 35 cycles, and a 10 min incubation period at 72 °C following the 35 cycles. Each cycle consisted of three steps: denaturation at 94 °C for 40 s, annealing at 55 °C for 30 s, and elongation at 72 °C for 30 s.

The purified DNA product from the second PCR, containing the altered MutT gene between the *Xba*I and *Bam*HI restriction sites, and the plasmid vector pET11b were digested with the *Xba*I and *Bam*HI restriction enzymes, ligated using T4 DNA ligase, and transformed into competent *E. coli* DH5α cells which were grown on LB/Amp (100 μg/mL) plates at 37 °C. Single colonies were screened for plasmids containing the inserted mutant gene by digesting plasmids, isolated from different colonies, with *Eco*RV. Agarose gel electrophoresis (0.7%) showed two bands with mobilities expected for the DNA fragments of 4229 and 1447 bp from the pET11b vector (no insert), while the vector containing the inserted gene exhibited bands with mobilities expected for the DNA fragments of 4229 and 1947 bp. Plasmids containing inserts were isolated and sequenced to verify the mutation and the otherwise unaltered DNA sequence. Subsequently, the verified mutated plasmid was transformed into *E. coli* DH5α cells for storage and future plasmid preparations and into *E. coli* HMS174 (DE3) cells for protein expression.

Overexpression and Purification of Recombinant Enzymes. Unlabeled, uniformly ^{15}N-labeled, and uniformly ^{15}N- and ^{13}C-labeled recombinant enzymes were expressed and purified as previously described (*17*) with the following additions or modifications. After being harvested, the cells (∼2.5 g/L) were lysed by resuspension in lysis buffer (10 mL of buffer/g of cells) [50 mM Tris-HCl buffer (pH 8.0) containing 5 mM EDTA, 10% sucrose, 1 mM dithiothreitol, 0.1% Triton X-100, and 0.1 mg/mL lysozyme] and stirring gently for 20 min followed by sonication. Fractions containing recombinant MutT enzymes from the Sephadex G-100 column were pooled and loaded directly onto a DEAE-Sepharose fast-flow column (35 cm × 2.5 cm) equilibrated with 50 mM Tris-HCl buffer (pH 7.5) and 20 mM NaCl. The purified enzymes eluted between 150 and 200 mM NaCl during a linear gradient from 20 to 250 mM NaCl in 50 mM Tris-HCl buffer (250 to 250 mL) (pH 7.5) at a rate of 2 mL/min. The enzyme preparations were concentrated by ultrafiltration, passed down a Sephadex G-25 column, equilibrated in 50 mM Tris-HCl buffer (pH 7.5), which had been passed over a Chelex-100 column, and stored at −80 °C before use in kinetic and metal binding studies. After passage over the Sephadex G-25 column, the uniformly ^{15}N-labeled mutants and the ^{15}N- and ^{13}C-labeled wild type MutT enzyme preparations were dialyzed against 1 mM d_{11}-Tris-HCl buffer (pH 7.5), lyophilized, and resuspended in 4 mM d_{11}-Tris-HCl buffer (pH 7.5) with 21 mM NaCl in H_2O/D_2O (90:10) before use in NMR studies. As determined by SDS−PAGE

and Coomassie Blue staining, the wild type and mutant enzymes were at least 98% pure.

Synthesis of [γ-^{32}P]dGTP. [γ-^{32}P]dGTP was prepared by transphosphorylation of dGDP from [γ-^{32}P]ATP catalyzed by bakers' yeast nucleoside diphosphate kinase (Sigma Chemical Co., St. Louis, MO). A 20 μL reaction mixture containing 50 mM Tris-HCl buffer (pH 7.5), 5 mM $MgCl_2$, 2.5 mM dGTP, 1.25 μM [γ-^{32}P]ATP (4×10^6 Ci/mol), and 3.4 units of kinase was incubated at 37 °C for 15 min. The reaction mixture was spotted on PEI-cellulose TLC plates (Aldrich) and developed in 0.6 M triethylammonium bicarbonate buffer (pH 8.0). Radioactive nucleotides were visualized by autoradiography, and the cellulose in the area of the TLC plate that contained [γ-^{32}P]dGTP was removed. [γ-^{32}P]-dGTP was eluted from the cellulose with 1 mL of 0.6 M triethylammonium bicarbonate buffer (pH 8.0), and the mixture was centrifuged. The supernatants from three washes were combined and lyophilized, and 500 μL of 15 mM dGTP was added to the lyophilized sample, yielding 15 mM [γ-^{32}P]-dGTP (5 Ci/mol).

Kinetic Studies. Steady-state kinetic experiments with either Mg^{2+}- or Mn^{2+}-activated mutant MutT enzymes were performed by measuring the amount of [^{32}P]pyrophosphate released from [γ-^{32}P]dGTP in 50 mM Tris-HCl buffer (pH 7.5) at 23 °C as described previously (*1*, *10*). The reactions in mixtures (50 μL) containing 1.4×10^{-3} to 5×10^{-2} mg/mL enzyme and varying concentrations of either $MgCl_2$ (0.2−32 mM) or $MnCl_2$ (0.2−12 mM) in the presence of [γ-^{32}P]dGTP (0.1−2 mM) were terminated by the addition of 100 μL of a solution containing 1 part 7% perchloric acid and 4 parts of a 20% suspension of Norit A. After being mixed and held on ice for 5 min, each sample was centrifuged and radioactivity was determined on a 60 μL aliquot of the supernatant. A unit of activity is 1 μmol of dGTP hydrolyzed/min. Under these conditions, the velocity of the reaction was linear with both time and enzyme concentration, not more than 10% of the substrate was hydrolyzed, and the lowest amount of [^{32}P]pyrophosphate product produced was more than twice that of background levels.

Effects of pH on k_{cat} of the Wild Type and Mutants of MutT. The pH dependence of k_{cat} for the dGTPase activity of wild type MutT and its E53Q, E53D, E44D, and K39Q mutants was determined by performing the kinetic assay described above over the indicated pH range at 37 °C using the following solution conditions. The buffers (50 mM each) and pH ranges that were used were sodium MES buffer (pH 5.5−7.0), Tris-HCl buffer (pH 7.0−9.0), and sodium CHES buffer (pH 9.0−10.5). At pH values below or above this range, irreversible inactivation of the wild type and mutant enzymes occurred. The reaction mixtures (50 μL) also contained either 20 or 30 mM $MgCl_2$ in the presence of either 3 or 6 mM [γ-^{32}P]dGTP and amounts of enzyme to yield a level of product formation of <10% in a time range of 10−30 min for wild type MutT (2.5×10^{-5} to 2.5×10^{-3} mg) and its E53D (0.01−0.1 mg), E44D (2.5×10^{-3} to 2.5×10^{-2} mg), and K39Q mutants (2×10^{-4} to 2×10^{-3} mg) and 30−120 min for the E53Q mutant (0.4 mg). The rates for the wild type- and mutant-catalyzed MutT reactions did not significantly vary with Mg^{2+} or [γ-^{32}P]dGTP concentration over the pH range that was studied, indicating that the measured rates for each enzyme were true k_{cat} values. A pH-stability curve was obtained for both the wild type and the E53Q mutant MutT by preincubating each enzyme at the indicated pH at 37 °C for times ranging from 1 to 3 times the duration of the assay and then measuring the activity at pH 7.5 and 37 °C.

Effects of Viscogenic Agents on k_{cat} of E53Q and Wild Type MutT. The dGTPase activities of wild type MutT and the E53Q mutant were measured in the presence of varying amounts of viscogen [0−40% (w/v) glycerol or sucrose] at 37 °C in 50 μL assay mixtures also containing 50 mM Tris-HCl buffer (pH 7.5), 20 mM $MgCl_2$, 3 mM [γ-^{32}P]dGTP, and either 5×10^{-5} mg of wild type MutT or 0.4 mg of E53Q mutant.

Mn^{2+} Binding Studies. The binding of Mn^{2+} by the mutant MutT enzymes was studied by EPR which directly measures the concentration of free Mn^{2+} in a mixture of free and bound Mn^{2+} (*22*) and by the enhancement of the paramagnetic effect of enzyme-bound Mn^{2+} on the longitudinal relaxation rate ($1/T_1$) of water protons, a property of bound Mn^{2+} (*23*). The concentrations of the mutant enzymes ranged from 0.3 to 0.9 mM, and that of $MnCl_2$ ranged from 0.25 to 2.5 mM. The solutions also contained 50 mM Tris-HCl buffer (pH 7.5), and the temperature was 22 °C. The EPR data were collected on a Varian E-4 EPR spectrometer (9.1 GHz) and analyzed as Scatchard plots as previously described for the wild type enzyme (*10*). The longitudinal relaxation rate of water protons was measured at 24.3 MHz, with a Seimco pulsed NMR spectrometer using a $180°-\tau-90°$ pulse sequence as previouly described (*23*). The enhancement factor (ϵ_b) was calculated as previously described for the wild type enzyme, correcting for the concentration of free Mn^{2+} which was independently determined by EPR (*10*). The solutions and conditions were identical to those used for the EPR studies.

Mg^{2+} Binding Studies. The stoichiometry and dissociation constants for Mg^{2+} binding to the mutants were determined by competition with Mn^{2+}. A solution containing 1.0 mM enzyme and 1.0 mM $MnCl_2$ in 50 mM Tris-HCl (pH 7.5) was titrated with an otherwise identical solution containing 70 mM $MgCl_2$ at 22 °C by monitoring the free Mn^{2+} by EPR and the bound Mn^{2+} by the observed enhancement (ϵ^*) of the paramagnetic effects of Mn^{2+} on $1/T_1$ of water protons as described in the preceding section. The titrations were fit by a computed hyperbolic curve which yielded an extrapolated minimum ϵ^*, reflecting the residual bound Mn^{2+}, and a concentration of free Mg^{2+} ($[Mg^{2+}]_F^{50}$) that gave half-maximal displacement of Mn^{2+}. The dissociation constant of Mg^{2+} was calculated from $[Mg^{2+}]_F^{50}$ using eq 2.

$$K_d^{Mg^{2+}} = \frac{[Mg^{2+}]_F^{50}}{\left(1 + \frac{[Mn^{2+}]_F^{50}}{K_d^{Mn^{2+}}}\right)} \quad (2)$$

In eq 2, $[Mn^{2+}]_F^{50}$ is the concentration of free Mn^{2+} at the half-point of the titration which was determined by both ϵ^* and EPR and $K_d^{Mn^{2+}}$ is the dissociation constant of Mn^{2+} determined as described in the preceding section.

General Heteronuclear NMR Methods. NMR samples contained either ^{15}N- and ^{13}C-labeled wild type MutT (1.4 mM) or ^{15}N-labeled E53Q (1.4 mM), E56Q (0.75 mM), or E44D (0.35 mM) mutant MutT enzyme, and 5 mM d_{11}-Tris-

HCl buffer (pH 7.5) in 600 μL of H_2O/D_2O (90:10). The NMR data were collected at 32 °C on a Varian Unity Plus 600 NMR spectrometer equipped with *z*-axis pulsed field gradient capabilities, using a Varian 5 mm triple-resonance probe. Water suppression for the three-dimensional NOESY experiment was achieved with a WATERGATE pulse train imediately before data acquisition (*24*) and for the three-dimensional TOCSY experiment by gradient selection (*25, 26*). Data were processed on a Silicon Graphics Indigo^2 XZ Workstation using the FELIX 2.3 software package (Biosym Technologies, Inc.). Multidimensional data sets were collected using the States−TPPI method (*25*) in all of the indirect dimensions, with relaxation delays of 0.9 s. Shifted (70°) sine bell filters were used in the first and subsequent dimensions, respectively, prior to zero-filling and Fourier transformation. The observed ^{1}H chemical shifts are measured with respect to the H_2O signal, which is 4.706 ppm downfield from external TSP at 32 °C, and are reported with respect to TSP. The ^{15}N chemical shifts are measured with respect to external $^{15}NH_4Cl$ (2.9 mM in 1 M HCl) at 20 °C, which is 24.93 ppm downfield from liquid ammonia (*27*), and are reported with respect to liquid ammonia.

Three-Dimensional $^1H-^{15}N$ NOESY-HSQC and Three-Dimensional $^1H-^{15}N$ TOCSY-HSQC Spectra of the E53Q, E56Q, and E44D MutT Mutants. Three-dimensional ^{1}H−^{15}N NOESY-HSQC experiments were performed on the ^{15}N-labeled mutant MutT solutions containing the other components as described above, with a 150 ms mixing time using the pulse sequence described previously (*11, 13*). The data were obtained at 600 MHz with spectral widths of 7200, 2000, and 8000 Hz in f_1 (^{1}H), f_2 (^{15}N), and f_3 (^{1}HN), respectively, and with 256, 72, and 1024 complex points, respectively, in the t_1, t_2, and t_3 dimensions. A total of eight transients were acquired for each hypercomplex t_1, t_2 pair. The final data matrix was 256 × 128 × 256 real points for the f_1 (^{1}H), f_2 (^{15}N), and f_3 (^{1}HN) dimensions, respectively.

Three-dimensional ^{1}H−^{15}N TOCSY-HSQC experiments were performed on the same samples using the pulse sequence described previously (*28*) and a spin lock time of 65 ms. The data were obtained at 600 MHz with spectral widths of 7200, 2000, and 8000 Hz in f_1 (^{1}H), f_2 (^{15}N), and f_3 (^{1}HN), respectively, and with 256, 72, and 1024 complex points, respectively, in the t_1, t_2, and t_3 dimensions. A total of eight transients were acquired for each hypercomplex t_1, t_2 pair. The final data matrix was 256 × 128 × 256 real points for the f_1 (^{1}H), f_2 (^{15}N), and f_3 (^{1}HN) dimensions, respectively.

Two-Dimensional CO(C)H Titrations of Wild Type MutT. Two-dimensional CO(C)H spectra, which correlate the chemical shifts of all carboxylate and carbonyl carbons with those of adjacent methylene or methine protons, were recorded at enzyme concentrations of 1.4 mM in samples containing 4 mM d_{11}-Tris-DCl (pH 7.5) and 21 mM NaCl in D_2O using the pulse sequence described previously (*12, 29*). The data were obtained at 600 MHz with spectral widths of 2242 and 7200 Hz in f_1 (^{13}C) and f_2 (^{1}H), respectively, and with 192 and 512 complex points, respectively, in the t_1 and t_2 dimensions. A total of 16 transients were acquired for each hypercomplex t_1 point with ^{1}H and ^{13}C carriers positioned at 4.706 and 43.0 ppm, respectively. The final data matrix was 256 × 256 real points for the f_1 (^{13}C) and f_2 (^{1}H) dimensions, respectively.

In titrations of MutT with Mg^{2+}, $MgCl_2$ was added stepwise to the enzyme solution and two-dimensional CO(C)H spectra were recorded. The concentrations of Mg^{2+} ranged from 0.25 to 10 mM in eight steps. This sample was subsequently titrated with a mixture of an equimolar amount of Mg^{2+} and AMPCPP covering the same concentration range.

$^1H-^{15}N$ HSQC Spectra and Titrations of the E53Q, E56Q, and E44D MutT Mutants. ^{1}H−^{15}N HSQC spectra were recorded for the ^{15}N-labeled mutant MutT solutions containing the other components as described above using the pulse sequence described previously (*26*). The data were obtained at 600 MHz with spectral widths of 2000 and 8000 Hz in f_1 (^{15}N) and f_2 (^{1}H), respectively, and with 256 and 1024 complex points, respectively, in the t_1 and t_2 dimensions. A total of eight transients were acquired for each hypercomplex t_1 point with ^{1}H and ^{15}N carriers positioned at 4.706 and 120.06 ppm, respectively. The final data matrix was 256 × 256 real points for the f_1 (^{15}N) and f_2 (^{1}H) dimensions, respectively.

^{1}H−^{15}N HSQC titrations of the ^{15}N-labeled mutant MutT solutions, containing the other components as described above, with Mn^{2+}, Mg^{2+}, and dGTP were performed as described previously (*13*). In titrations of enzyme with Mn^{2+}, $MnCl_2$ was added stepwise to the enzyme solution and the ^{1}H−^{15}N HSQC spectra were recorded. The concentrations of Mn^{2+} ranged from 0.4 to 56 μM in 15 steps. At each Mn^{2+} concentration, the intensity of the cross-peaks was measured by volume integration using the NMRVIEW 2.1 software package (*30*). In other titrations, $MgCl_2$ or dGTP was added stepwise to the enzyme solutions and ^{1}H−^{15}N HSQC spectra were recorded. The concentrations of Mg^{2+} ranged from 0.25 to 30 mM in 12 steps. The concentrations of dGTP ranged from 0.5 to 7.0 mM in seven steps.

Since the complexes of either Mg^{2+} or dGTP with the MutT mutants are in fast exchange on the chemical shift time scale (see Results and Discussion), the dissociation constant (K_d) and the amide ^{15}N and ^{1}H assignments for the complex of each mutant with either Mg^{2+} or dGTP were determined by titration of the enzyme with either Mg^{2+} or dGTP and following the changes in the ^{1}H and ^{15}N chemical shifts in a series of ^{1}H−^{15}N HSQC spectra obtained as described above. The absolute values of the chemical shift changes ($\Delta\delta_{obs} = |\delta_{free} - \delta_{complex}|$) for well-resolved resonances with significant $\Delta\delta_{max}$ values were plotted against the total concentration of either dGTP or Mg^{2+} (L_t). Such plots were used to determine K_d according to eq 3:

$$\Delta\delta_{obs} = \frac{\Delta\delta_{max}[(K_d + L_t + E_t) - \sqrt{(K_d + L_t + E_t)^2 - 4L_tE_t}]}{2E_t} \quad (3)$$

taking into account the small changes in total enzyme concentration, E_t, due to dilution of the NMR sample upon addition of ligand, by performing nonlinear least-squares regression analysis using both L_t and E_t as codependent variables. As found with the wild type enzyme (*13*), a stoichiometry of one ligand binding site is assumed. The percent occupancy at the binding site at a given L_t is obtained from the value of $\Delta\delta_{obs}/\Delta\delta_{max}$ calculated from eq 3 using the known values of K_d, L_t, and E_t.

Scheme 1

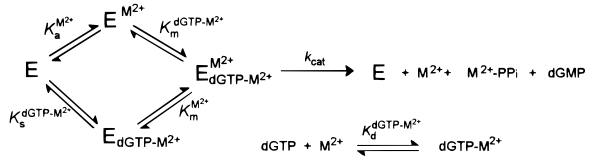

RESULTS AND DISCUSSION

Kinetic Properties of the Mutants of Glu-44, -53, -56, and -98 of the MutT Enzyme. It has been shown that wild type MutT follows the kinetic mechanism shown in Scheme 1 in which hydrolysis of the dGTP−M^{2+} substrate requires activation by both an enzyme-bound and a nucleotide-bound divalent metal cation (*10*). By varying both the metal and dGTP concentrations and measuring the initial reaction velocities, Frick et al. previously determined the five kinetic parameters defined in Scheme 1 for the wild type MutT-catalyzed reaction (Table 1) (*10*). The effects of mutating the conserved glutamate residues (Figures 1 and 2) on the five kinetic parameters for both the Mg^{2+}- and Mn^{2+}-activated enzymes were studied. The concentrations of free M^{2+} and of dGTP−M^{2+} were calculated for each point from the previously determined K_d (dGTP−Mg^{2+}) of 50 μM and K_d (dGTP−Mn^{2+}) of 10 μM (*10*, *31*).

If the rapid equilibrium assumption is made for M^{2+} and dGTP−M^{2+} binding, rate eq 4

$$v = (V_{max}[M^{2+}][dGTP{-}M^{2+}])/(\beta K_a^{M^{2+}} K_s^{dGTP-M^{2+}} + \beta K_a^{M^{2+}}[dGTP{-}M^{2+}] + \beta K_s^{dGTP-M^{2+}}[M^{2+}] + [M^{2+}][dGTP{-}M^{2+}]) \quad (4)$$

has been derived for the kinetic mechanism in Scheme 1 where β is a proportionality constant which when multiplied by $K_a^{M^{2+}}$ yields the value for $K_m^{M^{2+}}$ and when multiplied by $K_s^{dGTP-M^{2+}}$ yields the value for $K_m^{dGTP-M^{2+}}$ (*32*). A simultaneous fit of the data for each mutant, with both Mg^{2+} and Mn^{2+} activation, to eq 4 yielded the values of the five kinetic parameters defined in Scheme 1 (Table 1). The values for the kinetic parameters of Scheme 1 obtained with eq 4 agree within experimental error with those obtained by extrapolation from primary and secondary plots of the data as previously described for the wild type enzyme (*10*).

Mutants of Glu-53. The $10^{2.2}$- and $10^{2.6}$-fold decreases in k_{cat} found with the Mn^{2+}- and Mg^{2+}-activated E53D mutant, respectively, indicate that Glu-53 plays an important role in catalysis. In support of a major role for Glu-53, the isoelectronic E53Q mutation results in little or no catalytic activity with Mg^{2+} or Mn^{2+} as the activator under the standard conditions of 50 mM Tris-HCl buffer (pH 7.5) and 23 °C, indicating a loss of at least 10^5-fold in activity, based on the sensitivity of the radioactivity-based kinetic assay. The Mg^{2+}-dependent activity of the E53Q mutant could be measured at a higher temperature (37 °C). In comparison with the k_{cat} value for the wild type enzyme under these conditions, the value of k_{cat} decreased $10^{4.7}$-fold for the Mg^{2+}-activated reaction (Table 1). The greater loss of activity resulting from the E53Q mutation, compared to that from the E53D mutation, suggests that Glu-53 functions as a base in the active quaternary complex. Because of its low activity, no detailed kinetic analysis of the E53Q mutant was carried out.

With the E53D mutant, the 14-fold increase in $K_a^{Mn^{2+}}$ and the 2.5-fold increase in $K_a^{Mg^{2+}}$, in comparison with those of the wild type enzyme (Table 1), suggest that in the binary E−M^{2+} complex Glu-53 interacts with the enzyme-bound divalent cation either by direct coordination or by a second-sphere interaction. Similarly, the increased $K_m^{M^{2+}}$ values for the E53D mutant with both divalent cations (Table 1) suggest that in the active quaternary complex, as well, Glu-53 interacts with the enzyme-bound divalent cation. If Glu-53 functions as a general base, its carboxylate interaction in the quaternary complex must be in the second coordination sphere rather than in the inner sphere of the metal ion (Figure 2).

With Mn^{2+}-activated MutT, the E53D mutation increased the K_s and K_m values of dGTP−Mn^{2+}, while with the Mg^{2+}-activated enzyme, this same mutation decreased the K_s and K_m values of dGTP−Mg^{2+} (Table 1), suggesting structural differences in the ternary E−M^{2+}−dGTP and E−dGTP−M^{2+} and quaternary E−M^{2+}−dGTP−M^{2+} complexes of the two metal ions.

Mutants of Glu-56 and Glu-98. Although the four liganding mutants E56Q, E56D, E98Q, and E98D all resulted in reduced catalytic activity especially with Mg^{2+}, those of Glu-56 were more damaging to catalysis than those of Glu-98. The k_{cat} values of E56Q and E56D are 24- and 47-fold lower, respectively, than that of the wild type enzyme, while those of E98Q and E98D are only 6.3- and 5.6-fold lower, respectively. When these mutants were activated by Mn^{2+}, the k_{cat} values decreased by smaller factors of 1.5-, 4.4-, 1.7-, and 1.5-fold for E56Q, E56D, E98Q, and E98D, respectively.

For the E56Q, E56D, E98Q, and E98D mutants, the 2.2-, 1.1-, 1.5-, and 3.7-fold increases in $K_a^{Mg^{2+}}$, respectively, and the 3.8-, 2.4-, 1.5-, and 3.9-fold increases in $K_a^{Mn^{2+}}$, respectively, suggest weaker metal binding in the binary E−M^{2+} complexes of these mutants. Weaker metal binding is seen more clearly in the quaternary E−M^{2+}−dGTP−M^{2+} complex by $K_m^{M^{2+}}$ values of the free metal, at saturating levels of the dGTP−M^{2+} substrate. The $K_m^{Mg^{2+}}$ values increased 5.1-, 2.9-, 6.2-, and 8.8-fold with the E56Q, E56D, E98Q, and E98D mutants, respectively, while the $K_m^{Mn^{2+}}$ values increased 22-, 7.6-, 3.0-, and 12-fold, respectively. Thus, the kinetic data suggest that Glu-56 and Glu-98 contribute to metal binding in the quaternary E−M^{2+}−dGTP−M^{2+} complex much more than in the binary E−M^{2+} complex.

With respect to substrate binding by the wild type enzyme, the $K_s^{dGTP-M^{2+}}$ and $K_m^{dGTP-M^{2+}}$ values with wild type MutT provided reasonable approximations of the true dissociation constants of the dGTP−M^{2+} substrate from the free enzyme and from the E−M^{2+} complex, respectively (*10*). These approximations would be expected to apply to the mutants as well, since their k_{cat} values are lower, allowing more time for equilibration of the substrate and metals with the enzyme prior to catalysis. While the K_s values of the dGTP−Mg^{2+} complex decreased by an order of magnitude in the four liganding mutants, those of dGTP−Mn^{2+} increased by 1.8−3.9-fold, suggesting differing interactions of the two dGTP−M^{2+} complexes with the enzyme in their respective ternary complexes. In the active quaternary complexes of the

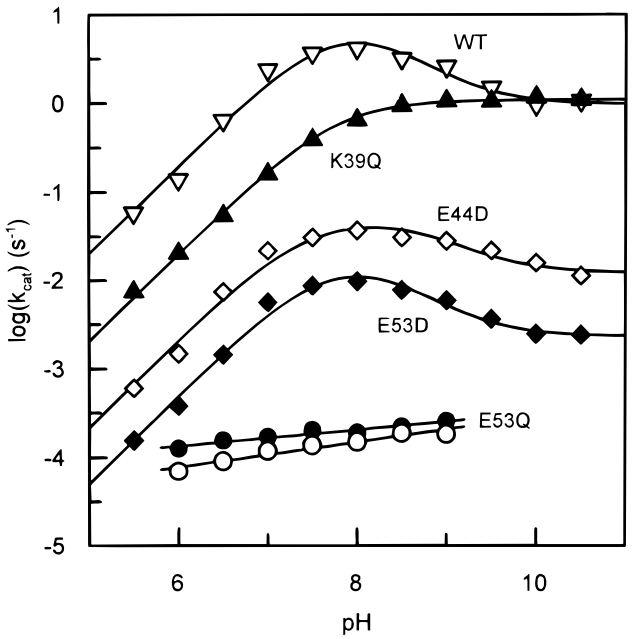

FIGURE 3: pH dependence of k_{cat} of wild type MutT (▽) and the following mutants: K39Q (▲), E44D (◇), E53D (◆), and E53Q before (○) and after (●) correction for pH-dependent denaturation effects. The curves were computed from nonlinear least-squares fits of the data as described in the text using the parameters given in Table 2.

mutants, with the exception of the E56Q and E98Q mutants in the presence of Mg^{2+}, the K_m values of the dGTP−M^{2+} complex generally increased in the liganding mutants from 2.2- to 9.4-fold, indicating weaker dGTP−M^{2+} binding.

Mutants of Glu-44. Despite the distance of Glu-44 from the active site (Figure 1), mutation of this residue to Gln or Asp produced effects on kinetic parameters similar to those of the liganding mutants of Glu-56 and Glu-98 (Table 1). Thus, in comparion with that of the wild type MutT, the k_{cat} values of Mg^{2+}-activated E44Q and E44D each decreased 1 order of magnitude more than did those of the Mn^{2+}-activated mutants. With both metal activators, the E44D mutant is kinetically more damaged than the E44Q mutant, suggesting that residue size, rather than charge, is important in the role of Glu-44. Both the E44Q and E44D mutations weakened metal binding in the quaternary complex but not in the binary E−M^{2+} complexes. In comparison with wild type MutT, substrate binding is weakened in the quaternary E−Mg^{2+}−dGTP−Mg^{2+} and E−Mn^{2+}−dGTP−Mn^{2+} complexes and in the ternary E−dGTP−Mn^{2+} complex, but tightened in the ternary E−dGTP−Mg^{2+} complex.

Effects of pH on k_{cat} of Wild Type MutT and Its E53Q, E53D, E44D, and K39Q Mutants. The question of whether Glu-53 functions as a general base in the active quaternary complex was further investigated by comparing the pH dependence of k_{cat} of wild type MutT with those of the E53Q, E53D, E44D, and K39Q mutants. For wild type MutT and the E53D and E44D mutants, plots of log(k_{cat}) versus pH exhibited a limiting slope of 1 on the ascending limb and then a hump, i.e., a sharply defined maximum near pH 8, followed by a plateau (Figure 3). The simplest model which fits these observations is shown in Scheme 2, where K_{H_2ES} and K_{HES} are the ionization constants for an *essential* base catalyst and a *nonessential* acid catalyst, respectively, in the active quaternary MutT−Mg^{2+}−dGTP−Mg^{2+} complex and

Scheme 2

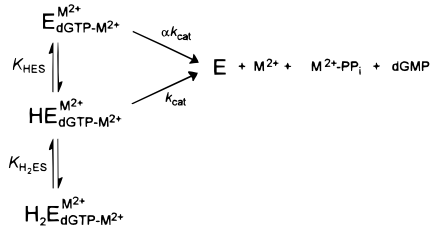

Table 2: Parameters Used To Fit the pH Dependence of k_{cat} for MutT and Its Mutants at 37 °C

enzyme	pK_{H_2ES}	pK_{HES}	$(k_{cat})^{max}$ (s^{-1})	α
wild type	7.7 ± 0.2	8.2 ± 0.4	9.2 ± 1.6	0.11 ± 0.01
E53Q			$(2.5 \pm 0.3) \times 10^{-4}$	
E53D	7.6 ± 0.2	8.3 ± 0.3	$(1.9 \pm 0.2) \times 10^{-2}$	0.12 ± 0.01
K39Q	7.7 ± 0.1		1.1 ± 0.2	
E44D	7.4 ± 0.2	8.8 ± 0.4	$(5.4 \pm 0.5) \times 10^{-2}$	0.22 ± 0.01

α is a proportionality constant relating k_{cat} for the reaction of the enzyme with the two different ionic forms of the acid catalyst. With the rapid equilibrium assumption, the pH dependence of k_{cat} is given by eq 5 (*32*):

$$k_{cat} = \frac{(k_{cat})^{max}\left(1 + \frac{\alpha K_{HES}}{[H^+]}\right)}{1 + \frac{[H^+]}{K_{H_2ES}} + \frac{K_{HES}}{[H^+]}} \quad (5)$$

From eq 5 (with $0 < \alpha < 1$), the maximum value of k_{cat}, $(k_{cat})^{max}$, occurs with the protonated form of the acid group, and the value of k_{cat} in the plateau region (pH >9) is that of the slower reaction with the unprotonated form of the acid group, resulting in a hump. A nonlinear least-squares fit of the pH dependence of k_{cat} for the wild type reaction to the logarithmic form of eq 5 gave a pK_{H_2ES} value of 7.7 ± 0.2 for the base catalyst and a pK_{HES} value of 8.2 ± 0.4 for the acid catalyst (Table 2). The value of the proportionality constant α (0.11 ± 0.01) determined from this analysis indicates that the $(k_{cat})^{max}$ value of 9.2 ± 1.6 s^{-1} of wild type MutT, which occurs when the acid group is in its protonated form, is 9.1 times larger than when it is unprotonated (k_{cat} = 1.0 s^{-1}).

The E53Q mutation, which results in a $10^{4.6}$-fold decrease in $(k_{cat})^{max}$ compared to that of the wild type (Table 2), also resulted in the loss of the pK_{H_2ES} at 7.7 for the base catalyst in the plot of log(k_{cat}) versus pH (Figure 3). In this plot, the observed slope of 0.14 ± 0.02 reflects an artifact in the assay due primarily to more extensive denaturation during the assay time at lower pH values since a pH-dependent first-order decay in the measured activity was observed over this pH range. By extrapolation to zero assay time, a significantly lower slope (0.092 ± 0.011) of the plot of log(k_{cat}) versus pH is obtained (Figure 3), suggesting that the true slope is zero. The replacement of Gln with Asp at position 53 in the E53D mutant restored the pH dependence of k_{cat} (Figure 3), yielding pK_{H_2ES}, pK_{HES}, and α values very similar to those of the wild type enzyme and a $(k_{cat})^{max}$ which was $10^{1.9}$-fold greater than that of the E53Q mutant (Table 2). The greater loss of activity resulting from the E53Q mutation, compared to that from the E53D mutation (Tables 1 and 2), the loss of

the pK_{H_2ES} of 7.7 in the pH dependence of k_{cat} with the E53Q mutant, and its restoration with the E53D mutant provide evidence that Glu-53 functions as a base catalyst in the MutT reaction. The pK_{H_2ES} value of 7.7 for Glu-53 in the quaternary MutT−Mg^{2+}−dGTP−Mg^{2+} complex is significantly higher than the pK_a of ∼4 which is expected for the side chain carboxyl group of an exposed glutamic acid residue, and could result from electrostatic attraction of the protonated carboxyl group by the adjacent triphosphate moiety of bound dGTP.

As indicated by 1/α, the (8.7 ± 0.4)-fold decreases in k_{cat} of the wild type and E53D mutant enzymes at high pH agree with the 8-fold decrease in k_{cat} which occurs as a result of the K39Q mutation (*14*) and are consistent with the acid catalyst being assigned to Lys-39, a residue appropriately positioned to interact with the leaving nucleoside monophosphate (Figure 2). In support of this role, the pH dependence of k_{cat} for the K39Q mutant shows no descending limb at high pH, but a plateau which overlaps the plateau obtained with the wild type enzyme (Figure 3). Analysis of these data with a simplified form of eq 5 in which both K_{HES} and α are set to zero, reflecting the requirement for only an essential base, yielded a pK_{H_2ES} of 7.7 ± 0.1 in agreement with that of the wild type enzyme and a $(k_{cat})^{max}$ which is 8.4-fold lower (Table 2). Thus, the loss of a positive charge at position 39, either by the deprotonation of Lys or by its substitution with Gln, decreases k_{cat} by the same factor of 8.7 ± 0.4. While alternative roles for Glu-53 and Lys-39 in catalysis cannot be totally excluded, the effects of pH on k_{cat} (Figure 3 and Table 2) together with the solution structure of the quaternary complex (Figure 2) strongly support their functioning as base and acid catalysts, respectively.

With the remote mutant, E44D, which was kinetically more damaged than E44Q, the pH dependence of k_{cat} paralleled that of the wild type enzyme with very similar values of pK_{H_2ES} and pK_{HES}, a $10^{2.2}$-fold decrease in $(k_{cat})^{max}$ and a 2-fold increase in α (Table 2), the latter reflecting a decreased sensitivity of k_{cat} to the deprotonation of Lys-39. Since both Lys-39 and Glu-44 are in loop I, and Glu-44 precedes helix I which contains several conserved residues (Figure 1), these effects suggest destabilization of loop I and helix I by the E44D mutation.

Solvent Viscosity Dependence of k_{cat} for Wild Type and E53Q Mutant MutT. The ascending limb of the pH profile of k_{cat} for the wild type MutT reaction with a slope of 1 (Figure 3), indicative of an essential base catalyst, shows chemistry to be at least partially rate-limiting. To independently test whether the loss of this ascending limb due to the E53Q mutation (Figure 3) results from the loss of the base catalyst or from a change in the rate-determining step, viscosity effects on k_{cat} were evaluated. For the MutT-catalyzed reaction, k_{cat} would include all kinetic steps leading from the hydrolysis reaction to product release. Alterations in the solution viscosity should affect only the diffusional steps such as release of either dGMP or PP_i−M^{2+}. However, values of k_{cat} of both wild type MutT and the E53Q mutant did not vary in the presence of the microviscogens glycerol or sucrose over the range of 0−40% (w/v), indicating that neither dGMP nor PP_i−M^{2+} release is rate-limiting in either reaction and that a chemical step is likely to be rate-limiting with both wild type and E53Q mutant enzymes.

Structural Properties of the E53Q, E56Q, and E44D Mutant Enzymes. It is important to determine whether major losses of catalytic activity, as in the E53Q, E56Q, and E44D mutants, are due to specific alteration of an important catalytic or metal-binding residue or due to the loss of native-like protein structure. The backbone amide ^{15}N and NH resonances of the E53Q, E56Q, and E44D mutants in two-dimensional $^1H-^{15}N$ HSQC spectra were assigned by comparison of cross-peaks of the backbone NH resonances, in three-dimensional $^1H-^{15}N$ NOESY- and TOCSY-HSQC spectra, to those of wild type MutT for which complete ^1H, ^{15}N, and ^{13}C chemical shift assignments have been made (*17*). The glutamine side chain NϵH_2 assignments for Gln-53 [$\delta(^{15}N) = 110.35$; $\delta(NH) = 6.16$ and 7.13 ppm] and Gln-56 [$\delta(^{15}N) = 113.60$; $\delta(NH) = 6.49$ and 7.54 ppm] in the E53Q and E56Q mutants, respectively, were made by analysis of the three-dimensional $^1H-^{15}N$ TOCSY- and NOESY-HSQC spectra. The $^1H-^{15}N$ NOESY-HSQC spectra of each mutant showed little change in NOE intensities for nearly all residues, indicating very similar overall conformations for the wild type and the E53Q, E56Q, and E44D mutant enzymes.

The $^1H-^{15}N$ HSQC spectrum of the most kinetically damaged E53Q mutant enzyme indicates that 96% of the backbone ^{15}N resonances are unshifted (i.e., are within the error limits of 0.5 ppm of those of the wild type enzyme) and 83% of the backbone NH resonances are unshifted (i.e., are within the error limit of 0.05 ppm of those of the wild type enzyme) (Figures 4 and 5A). While the overall three-dimensional fold is preserved in the E53Q mutant, selective small changes in the ^{15}N and/or NH chemical shifts resulting from the E53Q mutation were observed for Gly-37, Lys-39, Glu-47, Ala-49, and Val-58 (Figure 4). The solution structure of the wild type enzyme (*11*) shows that all of these residues are located near the active site and are in proximity to the site of mutation (Figure 5A).

The previously reported failures by Lin et al. (*12*) to detect correlations involving the δ-carboxylate of Glu-53 in two-dimensional CO(C)H spectra either in free wild type MutT or in the quaternary MutT−Mg^{2+}−AMPCPP−Mg^{2+} complex over the temperature range of 14−41 °C and the pH range of 7.6−9.5 were confirmed in this study. In addition, no correlations involving the δ-carboxylate of Glu-53 were detected in a two-dimensional CO(C)H titration of the free enzyme with $MgCl_2$ alone at 32 °C. Thus, the side chain of Glu-53 likely exhibits conformational heterogeneity in the free enzyme, the binary E−Mg^{2+} complex, and the quaternary MutT−Mg^{2+}−AMPCPP−Mg^{2+} complex.

The two-dimensional $^1H-^{15}N$ HSQC spectrum of one of the most kinetically damaged metal-liganding mutants, E56Q, was similar to that of the wild type enzyme, with 90% of the residues exhibiting unaltered backbone ^{15}N chemical shifts (<0.5 ppm) and 92% of the residues exhibiting unaltered NH chemical shifts (<0.05 ppm), indicating that the overall backbone structure is largely intact. Residues with altered backbone ^{15}N or NH chemical shifts (Figure 5B) were widely distributed in the protein, including residues near the site of mutation: Leu-4 (in β-strand A), Glu-44 (in loop I), Gln-56, Val-58, and Gly-59 (in helix I), His-79 and Thr-81 (in β-strand D), Gly-96, Glu-98, Gly-99, Gln-100, and Gly-102 (in loop III), and Gly-109 (in loop IV). As found with the E57Q (*13*) and E53Q mutants, the E56Q mutation,

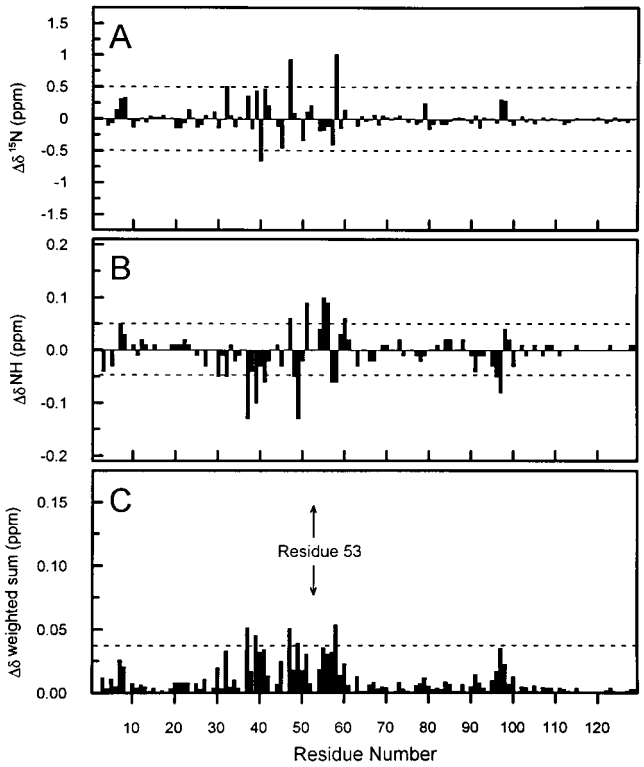

FIGURE 4: Backbone ^{15}N and NH chemical shift differences between wild type MutT and the E53Q mutant enzymes. Chemical shift differences ($\Delta\delta = \delta_{wildtype} - \delta_{mutant}$) were calculated on the basis of the chemical shift values obtained from ^{1}H−^{15}N HSQC spectra and plotted vs residue number. (A) ^{15}N chemical shift differences. (B) NH chemical shift differences. (C) Sum of the absolute magnitudes of the ^{15}N and NH chemical shift changes which were weighted according to the backbone amide chemical shift dispersion in the ^{15}N and ^{1}H dimensions (28.41 and 3.37 ppm, respectively) of the wild type enzyme's spectra. The dashed lines indicate the error limits.

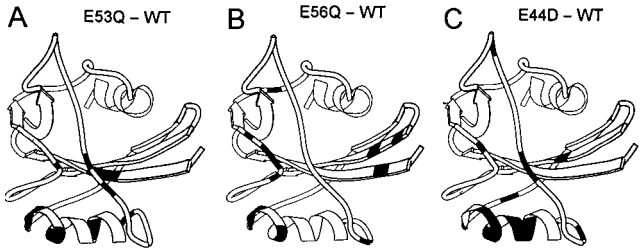

FIGURE 5: Sites of backbone ^{15}N and/or NH chemical shift differences from wild type MutT (shaded in black) in ^{1}H−^{15}N HSQC spectra of the following mutations: (A) E53Q, (B) E56Q, and (C) E44D.

presumably because of a loss of a negative charge, produced changes in chemical shifts in the same region of MutT as those produced by Mg^{2+} binding to the wild type enzyme.

The E44D mutant, the more kinetically damaged remote mutant, exhibited unaltered chemical shifts from wild type in 85% of the backbone ^{15}N resonances and in 74% of the backbone NH resonances, indicating a somewhat altered protein fold. Unlike the E56Q, E53Q, and E57Q mutants (*13*), the E44D mutation produced changes in chemical shifts more restricted to loop I and helix I (Figure 5C), involving Ala-30, Gly-37, and Thr-45 (in loop I) and Gln-48, Val-51, Arg-52, Glu-53, Glu-56, and Glu-57 (in helix I). Smaller shift changes occurred at Phe-65 (in loop II), Trp-83 (in β-strand D), and Gln-100 (in loop III). Thus, mutation of Glu-44, by altering the structure of loop I which immediately precedes helix I (residues 47−59) (Figure 1), destabilizes helix I.

Mn^{2+} Binding Studies. To independently study the binary E−Mn^{2+} complexes, seven of the eight glutamate mutants described here were titrated with $MnCl_2$. At each point of the titration, the enhancement (ϵ*) of $1/T_{1p}$ of water protons was determined by pulsed NMR and the free Mn^{2+} concentration was measured by EPR spectroscopy. With the wild type enzyme (*10*), Mn^{2+} binding studies by EPR revealed 0.9 ± 0.1 Mn^{2+} binding site with a dissociation constant $K_d^{Mn^{2+}}$ of 0.13 ± 0.04 mM (Table 3). With the E53D mutant, a Scatchard plot based on the EPR data shows that this mutant binds Mn^{2+} much more weakly at 2.7 ± 0.3 sites each with a $K_d^{Mn^{2+}}$ of 3.5 ± 0.3 mM (Figure 6A and Table 2). The $K_d^{Mn^{2+}}$ value agrees well with the kinetically determined value for $K_a^{M^{2+}}$ of 3.3 ± 0.6 mM for activation of the E53D mutant with Mn^{2+} (Table 1), indicating active site binding by at least one of the Mn^{2+} ions. The Scatchard plot in Figure 6B shows that the E53Q mutant also binds Mn^{2+} at 3.2 ± 1.0 sites with a dissociation constant $K_d^{Mn^{2+}}$ of 4.7 ± 0.9 mM (Table 3). Hence, the E53D and E53Q mutations result in 27- and 36-fold weaker Mn^{2+} binding compared to that of wild type MutT, indicating that Glu-53 interacts with the metal in the binary E−M^{2+} complex. At the high levels of Mn^{2+} required to populate the active site, nonspecific Mn^{2+} binding at approximately two additional sites was also detected.

Table 3 summarizes the results of titrations of the other five mutants with Mn^{2+}, analyzed by Scatchard plots of the EPR data. The binding stoichiometries of Mn^{2+} with the five mutants (Table 3) are very similar to those of the wild type enzyme, indicating one tight Mn^{2+} binding site for these mutants, with dissociation constants that are comparable to the kinetically determined activator constants of Mn^{2+} (Table 1). In comparison with those of the wild type enzyme, the dissociation constants of Mn^{2+} from the E56Q and E56D mutants increased by 3.5- and 1.7-fold, respectively, while those from the E98Q and E98D mutants were unaltered, suggesting that in the binary E−Mn^{2+} complex Glu-56 is a ligand while Glu-98 is not.

With the exceptions of the E56Q and E44D mutants, the enhancement factors of $1/T_{1p}$ of water protons (ϵ_b) resulting from Mn^{2+} binding to the other four mutants are significantly lower than that of the wild type enzyme, indicating structural changes in the coordination sphere of enzyme-bound Mn^{2+} in the E53Q, E53D, E56D, and E98D mutants (Table 3). In principle, such decreases in ϵ_b in these mutants could have resulted from either a decrease in the number of fast exchanging water ligands on the enzyme-bound Mn^{2+} or a decrease in the correlation time for the Mn^{2+}−water dipolar interaction which is dominated by the electron spin relaxation time of Mn^{2+} (*33*). Since the former is unlikely to result from the removal or weakening of a ligand from the protein by mutation, the latter alternative is more likely. A decrease in the dipolar correlation time can result from a decrease in the symmetry and/or rigidity of the ligands surrounding the enzyme-bound Mn^{2+} (*33*−*35*). From the ϵ_b values, these changes are greater in the kinetically most damaged E53Q mutant. A similarly decreased ϵ_b value of 8 ± 2 was observed with the liganding E57Q mutant of MutT which was comparably damaged kinetically (*13*).

Table 3: Comparison of Metal and Substrate Binding Properties of Mutants of MutT with Those of the Wild Type Enzyme

enzyme	complex	$n^{M^{2+}}$ (sites)	$K_d^{M^{2+}}$ (μM)	K_d (μM)	ϵ_b	ϵ_t	ϵ_q
wild type	(E−Mn^{2+})[a,b]	0.9 ± 0.1	130 ± 40		17.0 ± 1.7		
	(E−Mn^{2+}−AMPCPP−Mn^{2+})[b,c]	2.0 ± 0.1	16 ± 2			4.7 ± 0.5	8.7 ± 1.4
	E−Mg^{2+}		7500 ± 1200[b,d]	1450 ± 200[e,f]			
	E−dGTP			3440 ± 280[f,g]			
E44D	(E−Mn^{2+})[a]	1.1 ± 0.2	170 ± 10		15.3 ± 1.9		
	(E−Mn^{2+}−AMPCPP−Mn^{2+})[c]	2.0 ± 0.2				1.0 ± 0.5	9.5 ± 0.9
	E−Mg^{2+}		3120 ± 260[d]	1500 ± 200[e]			
	E−dGTP			600 ± 200[g]			
E53Q	(E−Mn^{2+})[a]	3.2 ± 1.0	4700 ± 900		8.1 ± 0.6		
	E−Mg^{2+}	1.0 ± 0.1[d]	21000 ± 4000[d]	15000 ± 2000[e]			
	E−dGTP			480 ± 50			
E53D	(E−Mn^{2+})[a]	2.7 ± 0.3	3500 ± 300		11.3 ± 1.1		
	(E−Mg^{2+})[d]	1.0 ± 0.1	31000 ± 4000				
E56Q	(E−Mn^{2+})[a]	1.4 ± 0.2	610 ± 70		15.2 ± 1.5		
	(E−Mn^{2+}−AMPCPP−Mn^{2+})[c]	2.0 ± 0.2				1.8 ± 0.1	5.4 ± 0.3
	E−Mg^{2+}		16000 ± 2000[d]	46000 ± 18000[e]			
	E−dGTP			970 ± 420[g]			
E56D	(E−Mn^{2+})[a]	1.1 ± 0.1	250 ± 30		13.7 ± 1.6		
	(E−Mn^{2+}−AMPCPP−Mn^{2+})[c]	2.0 ± 0.2	39 ± 4			2.6 ± 0.5	6.3 ± 1.6
	(E−Mg^{2+})[d]		10600 ± 1300				
E98Q	(E−Mn^{2+})[a]	1.1 ± 0.1	160 ± 10		10.8 ± 0.7		
	(E−Mn^{2+}−AMPCPP−Mn^{2+})[c]	2.2 ± 0.2				2.0 ± 0.1	5.7 ± 0.3
	(E−Mg^{2+})[d]		8000 ± 400				
E98D	(E−Mn^{2+})[a]	1.1 ± 0.2	160 ± 10		11.0 ± 0.5		
	(E−Mn^{2+}−AMPCPP−Mn^{2+})[c]	2.2 ± 0.1	39 ± 4			2.4 ± 0.2	5.5 ± 0.7
	(E−Mg^{2+})[d]		9800 ± 600				

[a] Determined by titration of the free enzyme with $MnCl_2$ at 23 °C and monitoring the binding of Mn^{2+} by the increase in the observed enhancement (ϵ^*) of $1/T_1$ of water protons, and independently by the disappearance of free Mn^{2+} by EPR. [b] From ref *10*. [c] Determined by titration of the E−AMPCPP complex with $MnCl_2$ at 23 °C and monitoring the binding of Mn^{2+} by the increase in the observed enhancement (ϵ^*) of $1/T_1$ of water protons. [d] Determined by titration of the enzyme−Mn^{2+} complex with $MgCl_2$ at 23 °C and monitoring the displacement of bound Mn^{2+} by the decrease in the observed enhancement (ϵ^*) of $1/T_1$ of water protons, and independently by the appearance of free Mn^{2+} by EPR. [e] Determined by $^1H-^{15}N$ HSQC titration of the enzyme with $MgCl_2$ at 32 °C. The stoichiometry (n) is assumed to be 1. [f] From ref *13*. [g] Determined by $^1H-^{15}N$ HSQC titration of the enzyme with dGTP at 32 °C. The stoichiometry (n) is assumed to be 1.

In contrast to the liganding mutants, the more remote mutant, E44D, exhibits an ϵ_b value (15.3 ± 1.9) which overlaps with that of the wild type enzyme (17.0 ± 1.7), and binds Mn^{2+} with the same affinity as the wild type (Table 3), indicating no significant change at the metal binding site in this mutant.

$^1H-^{15}N$ HSQC Titration of the E53Q Mutant Enzyme with $MnCl_2$. The locations of the three Mn^{2+} binding sites on the E53Q mutant were determined by titrating the enzyme with $MnCl_2$, and monitoring the attenuation of the assigned backbone NH and side chain NH_2 cross-peaks in $^1H-^{15}N$ HSQC spectra (Figure 7). This attenuation results from distance-dependent paramagnetic effects of Mn^{2+} on the longitudinal ($1/T_1$) and transverse ($1/T_2$) relaxation rates of the ^{15}N and NH resonances (*13*, *36*). The extent of attenuation of each cross-peak by Mn^{2+} is conveniently expressed as the concentration of Mn^{2+} which halves the intensity of each signal, $[Mn^{2+}]_{50}$ (Table 3). As previously shown (*36*), these $[Mn^{2+}]_{50}$ values when corrected by multiplication by the initial relative intensity of each cross-peak, to ensure equal paramagnetic effects on transverse relaxation rates ($1/T_{2p}$) for each affected NH cross-peak, yield $[Mn^{2+}]_{50}^{corr}$ values which are proportional to the relative (distance)^6 between Mn^{2+} and each attenuated $^{15}N-^1H$ vector (Tables 4 and 5). Because this analysis neglects paramagnetic effects of Mn^{2+} on $1/T_1$ of the affected ^{15}N and NH signals, which are much smaller but which also attenuate cross-peaks by decoupling (*37*), structural conclusions based on this analysis are only approximate (*36*).

With wild type MutT, the backbone NH resonances that were most attenuated by the presence of Mn^{2+} included Gly-37, Gly-38, and Lys-39 in loop I, Glu-53, Glu-56, Glu-57, and Val-58 in helix I, and Glu-98 in loop III (Table 4 and Figure 8A) (*13*). Figure 8A shows these residues are located in the active site of MutT. Quantitatively (Table 4), the $[Mn^{2+}]_{50}^{corr}$ values increased in the following order: K39 < G38 < E53 < E57 < E98 < G37 < E56 < V58, over a 6.4-fold range; this order reflects the progressively increasing relative distances from bound Mn^{2+} over a ∼1.4-fold range of distances. These residues also exhibited significant changes in the chemical shifts of their backbone NH resonances upon titration with Mg^{2+} (*13*).

With the E53Q mutant, HSQC titration with $MnCl_2$ also showed a pattern of disappearance of cross-peaks of active site residues similar to those seen in the wild type enzyme, but also showed Mn^{2+} binding at two additional sites located in β-turn I and loop IV (Figure 8B). The strongest effects were observed on the active site NH resonances of Gly-37, Gly-38, and Lys-39 in loop I and of Gln-53 (side chain NϵH_2) and Glu-57 in helix I (Figure 7A). Other residues at or near the active site that were affected include Gln-53, Glu-56, and Val-58 in helix I and Lys-97, Glu-98, Gly-99, and Gln-100 (side chain NϵH_2) in loop III (Figure 7B). For residues at or near the active site, the $[Mn^{2+}]_{50}^{corr}$ values (Table 4) increased in the following order: Q53 NϵH_a < Q53 NϵH_b < G37 < K39 < G38 < E57 < Q100 NϵH_a < Q100 NϵH_b < V58 < E98 < E56 < Q53 < K97 < G99, over a 40-fold range; this order reflects the closest interaction of Mn^{2+} with the side chain of the mutated residue Gln-53 and progressively increasing relative distances from bound Mn^{2+} to the other active site residues over a ∼1.9-fold range of distances. This order of effects differs from that found with wild type

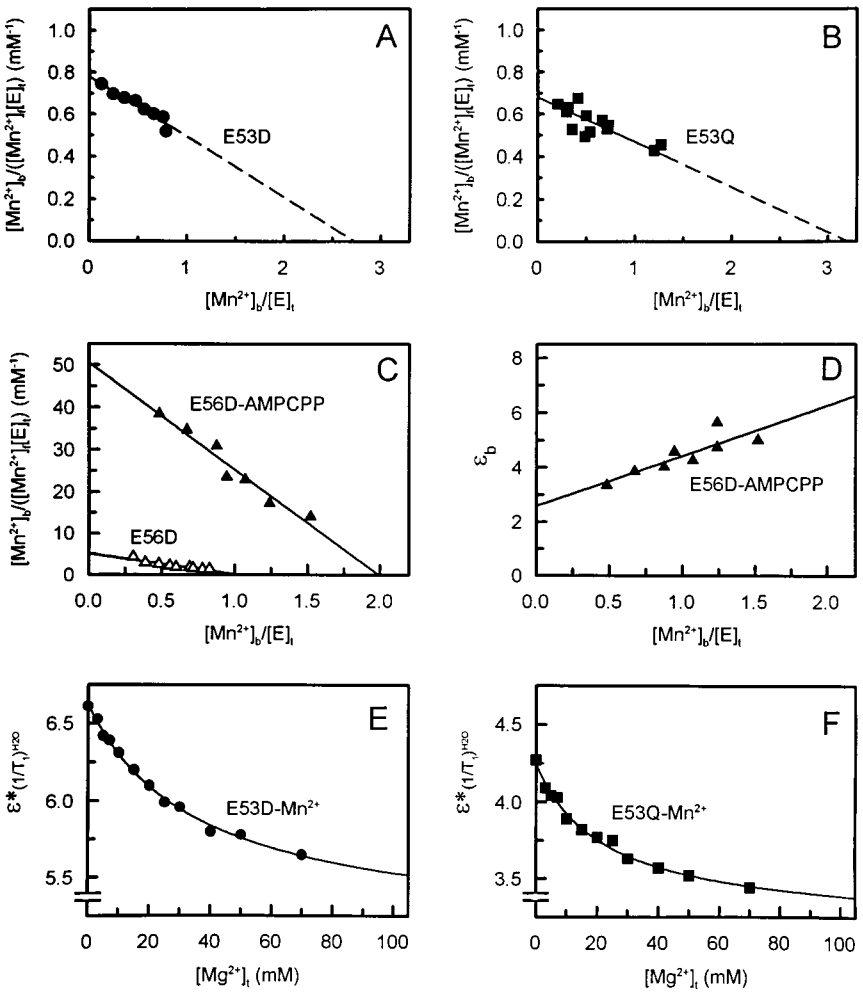

FIGURE 6: Metal binding by the E53D, E53Q, and E56D mutants of MutT. Scatchard plots of Mn^{2+} binding by (A) the E53D mutant (0.60 mM) and (B) the E53Q mutant of MutT (0.90 mM). (C) Scatchard plots of Mn^{2+} binding to E56D (0.41 mM, △) and to the E56D−AMPCPP complex (each 26 μM, ▲). (D) Enhancement of $1/T_1$ of water protons caused by bound Mn^{2+} (ϵ_b) as a function of Mn^{2+} site occupancy in the E56D−AMPCPP complex. Displacement by Mg^{2+} of Mn^{2+} from complexes of (E) the E53D mutant (1.0 mM) and (F) the E53Q mutant (1.0 mM) with Mn^{2+} (1.0 mM) by Mg^{2+}. In the titrations with $MgCl_2$, the concentrations of all other components were held constant. The other component present was 50 mM Tris-HCl (pH 7.5) at 23 °C. The concentrations of free Mn^{2+} were determined by EPR, and ϵ_b was determined by PRR correcting for free Mn^{2+} by EPR as described in Experimental Procedures.

MutT (Table 4), indicating that in the E53Q mutant, Mn^{2+} moves toward the backbone NH of Gly-37 and away from the backbone NHs of Glu-53, -56, -57, and -98. This change in the position of Mn^{2+} relative to its active site ligands in the E53Q mutant is also indicated quantitatively by the ratios of $([Mn^{2+}]_{50}^{corr})^{1/6}$ values for the mutant and wild type enzymes for each liganding residue (Table 5). These ratios, which reflect the relative distances from bound Mn^{2+} to backbone N−H vectors in the mutant and wild type enzyme, show a 7% decrease in the distance to Gly-37, and increases in the distance ranging from 20 to 66% to Glu-57 and Glu-53, respectively. Such a change in the position of the active site metal could contribute to the $10^{4.7}$-fold decrease in k_{cat} observed with the E53Q mutant (Table 1).

The two additional Mn^{2+} binding sites on the E53Q mutant detected by the HSQC titrations with Mn^{2+} are near loop IV and β-turn I (Table 4 and Figure 8B). Residues in loop IV with backbone or side chain NH resonances affected by Mn^{2+} binding include Asn-111 (side chain NδH$_2$), Asp-113, and Asp-114 (Figure 7C). Similarly, the Mn^{2+} binding site near β-turn I affects the side chain NδH$_2$ resonances of Asn-13 and Asn-15 (Figure 7D) whose side chain carbonyl groups may provide weak ligands to Mn^{2+} (Table 4).

Ternary and Quaternary Mn^{2+} and AMPCPP Complexes of the Mutants. The E56Q, E56D, E98Q, E98D, and E44D mutants, like the wild type enzyme, showed only one tight Mn^{2+} binding site. These mutants were further studied by Mn^{2+} binding to their respective E−AMPCPP complexes. Titration of the AMPCPP complex of the E56D mutant with Mn^{2+} (Figure 6C) yielded a stoichiometry of 2.0 ± 0.2 Mn^{2+} binding sites, indicating that, like the wild type enzyme, the E56D−AMPCPP complex binds two Mn^{2+} ions tightly with an average dissociation constant (39 ± 4 μM, Table 3) that is 2.4-fold weaker than that of the corresponding complex of wild type MutT (16 ± 2 μM, Table 3) and 5-fold tighter than the $K_m^{Mn^{2+}}$ (200 ± 10 μM, Table 1). A plot of the enhancement factor due to bound Mn^{2+} (ϵ_b) versus Mn^{2+} site occupancy (Figure 6D) showed a linear increase of ϵ_b with occupancy. The average enhancement for the quaternary E56D−Mn^{2+}−AMPCPP−Mn^{2+} complex (ϵ_q) is 6.3 by linear extrapolation to a site occupancy of 2.0. The average enhancement (ϵ_t) of either possible ternary complex, E56D−Mn^{2+}−AMPCPP or E56D−AMPCPP−Mn^{2+}, is 2.6 by linear extrapolation of ϵ_b to zero site occupancy (Table 3). These values of ϵ_q and ϵ_t are significantly lower than those of the wild type enzyme which were 8.7 and 4.7, respectively

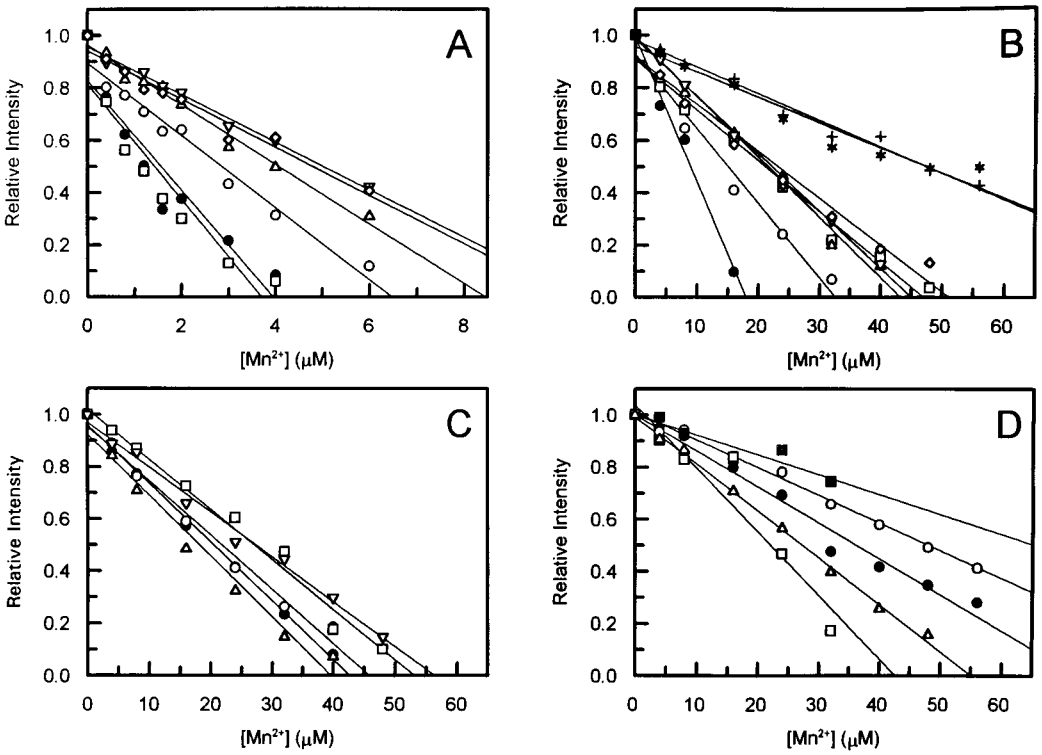

FIGURE 7: Comparison of paramagnetic effects as a function of Mn^{2+} concentration on the intensities of the backbone and side chain NH signals in $^1H-^{15}N$ HSQC spectra of the E53Q mutant MutT enzyme. The intensity of each peak was normalized using the C-terminal NH signal, which is uneffected by Mn^{2+}, as a reference. (A) Active site residues most strongly affected [Q53 NϵH$_a$ (●), Q53 NϵH$_b$ (○), G37 (□), E57 (△), G38 (▽), and K39 (◇)]. (B) Other active site residues [Q100 NϵH$_a$ (●), Q100 NϵH$_b$ (○), E98 (□), E56 (△), V58 (▽), Q53 (◇), G99 (+), and K97 (*)]. (C) Residues in the second Mn^{2+} binding site located in loop IV [N111 NϵH$_a$ (●), N111 NϵH$_b$ (○), D113 (□), D114 (△), and N111 (▽)]. (D) Residues in the third Mn^{2+} binding site located in β-turn I [N15 NϵH$_a$ (●), N15 NϵH$_b$ (○), N13 NϵH$_a$ (■), N13 NϵH$_b$ (□), and G92 (△)].

(Table 3), reflecting alterations in the inner coordination spheres of one or both of the bound Mn^{2+} ions.

Similar stoichiometries of approximately two tight Mn^{2+} binding sites were found with the AMPCPP complexes of the E56Q, E98Q, E98D, and E44D mutants (Table 3). However, due to interference by the weaker binding of Mn^{2+} to additional sites, dissociation constants could not be accurately determined. As with the E56D mutant, the ϵ_q and ϵ_t values of the other liganding mutants, E56Q, E98Q, and E98D, were much lower than those of the wild type enzyme, indicating an altered coordination sphere of one or both Mn^{2+} ions. In contrast, with the E44D remote mutant, the ϵ_q value overlapped with that of the wild type enzyme, indicating intact metal binding sites in the quaternary complex. The decreased ϵ_t value, however, indicates an altered metal enviroment in the ternary E44D−Mn^{2+}−AMPCPP complex.

Mg^{2+} Binding Studies by Competition with Mn^{2+}. The dissociation constants for Mg^{2+} binding to the E53Q, E53D, E56Q, E56D, E98Q, E98D, and E44D mutants were determined by titration of the E−Mn^{2+} complexes with $MgCl_2$ by monitoring the displacement of bound Mn^{2+} by the decrease in the observed enhancement (ϵ*) of $1/T_1$ of water protons, and independently by the appearance of free Mn^{2+} by EPR. With the E53D mutant, the addition of Mg^{2+} up to a final concentration of 70 mM displaced only 26% of the bound Mn^{2+}. Computer fitting the data to a titration curve (Figure 6E) indicated that saturating Mg^{2+} displaces only 32% of the bound Mn^{2+}, indicating that only one of the three binding sites for Mn^{2+} was readily occupied by Mg^{2+} over the concentration range that was used, and that the value of ϵ_b is similar for all Mn^{2+} binding sites. The dissociation constant for Mg^{2+} (31 ± 4 mM) determined from the half-point of the computed titration curve (Figure 6E and Table 3) agrees well with the kinetically determined activator constant of 36 ± 6 mM (Table 1), indicating that this Mg^{2+} is bound at the active site.

Very similar behavior was found with the E53Q mutant (Figure 6F) with which saturating Mg^{2+} also displaced 32% of the bound Mn^{2+}, indicating that only one of the three Mn^{2+} binding sites was readily occupied by Mg^{2+}, yielding a dissociation constant for Mg^{2+} from this site of 21 ± 4 mM. Although the activator constant of Mg^{2+} could not be determined with the E53Q mutant because of its low catalytic activity, the binding of Mg^{2+} occurs at the active site as found by direct $^1H-^{15}N$ HSQC titration of the E53Q mutant with $MgCl_2$ (see below).

Thus, with both the E53D and E53Q mutants, Mn^{2+} binding occurs with approximately equal affinity at three sites (Figure 6A,B), one of which is the active site (Figure 8B). In contrast, Mg^{2+} binds preferentially to the active site, with no detectable binding at the two additional sites. Such selectivity in active site binding by Mg^{2+} is consistent with its biological role as the predominant intracellular divalent cation activator of metal-requiring enzymes. While transition metal ions usually bind more tightly than Mg^{2+} to active sites of metal-requiring enzymes (Tables 1 and 3), they also bind with much greater affinity to other sites, often resulting in enzyme inhibition.

Table 4: Concentrations of Mn^{2+} Required To Decrease HSQC Cross-Peak Intensities by 50% ($[Mn^{2+}]_{50}^{corr}$) for Various Backbone and Side Chain Amide Resonances of the Wild Type and the E53Q Mutant of MutT

enzyme (binding site)	residue	resonance	secondary structure location	chemical shift (ppm) ^1H	chemical shift (ppm) ^{15}N	$[Mn^{2+}]_{50}$ (μM)	initial relative peak volume	$[Mn^{2+}]_{50}^{corr}$ (μM)
wild type (active site)	Lys-39	NH	loop I	8.29	121.95	2.30	1.57	3.60
	Gly-38	NH	loop I	8.52	106.59	2.80	2.40	6.72
	Glu-53	NH	helix I	8.85	118.11	6.20	2.19	7.05
	Glu-57	NH	helix I	8.82	116.62	4.67	1.92	8.96
	Glu-98	NH	loop III	8.69	123.64	10.3	1.10	11.3
	Gly-37	NH	loop I	8.1	109.79	5.25	2.31	12.1
	Glu-56	NH	helix I	8.19	119.81	6.50	1.97	12.8
	Val-58	NH	helix I	7.38	111.93	12.0	1.92	23.0
E53Q (active site)	Gln-53	NϵH$_a$	helix I	6.16	110.35	1.57	3.05	4.78
		NϵH$_b$	helix I	7.13	110.35	2.86	2.60	7.45
	Gly-37	NH	loop I	8.19	109.26	1.43	5.43	7.76
	Lys-39	NH	loop I	8.35	121.34	5.02	3.09	15.5
	Gly-38	NH	loop I	8.52	106.57	4.79	5.15	24.7
E53Q (active site)	Glu-57	NH	helix I	8.84	116.85	4.07	6.48	26.4
	Gln-100	NϵH$_a$	loop III	6.95	113.81	8.97	5.63	50.6
		NϵH$_b$	loop III	7.58	113.81	15.1	4.03	60.8
	Val-58	NH	helix I	7.40	110.75	22.2	4.32	96.0
	Glu-98	NH	loop III	8.61	123.18	21.1	5.74	121
	Glu-56	NH	helix I	8.06	119.75	21.6	5.98	129
	Gln-53	NH	helix I	8.88	117.16	23.2	6.22	145
	Lys-97	NH	loop III	7.81	121.93	47.5	3.14	149
	Gly-99	NH	loop III	8.54	113.35	47.5	3.99	190
E53Q (loop IV)	Asn-111	NδH$_a$	loop IV	6.92	114.81	21.8	3.89	84.9
		NδH$_b$	loop IV	7.55	114.81	20.5	4.47	91.5
	Asp-114	NH	loop IV	7.88	118.97	18.2	5.51	100
	Asn-111	NH	loop IV	9.42	124.98	27.3	5.32	146
	Asp-113	NH	loop IV	8.35	117.42	27.1	6.49	176
E53Q (β-turn I)	Asn-13	NδH$_a$	β-turn I	5.45	114.18	22.1	1.49	33.0
		NδH$_b$	β-turn I	7.74	114.18	65.6	1.00	65.6
	Gly-92	NH	loop III	8.60	115.28	27.3	5.18	142
	Asn-15	NδH$_a$	β-turn I	6.71	114.34	36.2	4.11	149
		NδH$_b$	β-turn I	7.16	114.34	48.1	3.99	192

Table 5: Relative Changes in the Distance from Various Backbone NH Groups to Enzyme-Bound Mn^{2+} in the Binary Mn^{2+}−MutT Complex as a Result of the E53Q Mutation

residue	resonance	secondary structure location	$^{WT}[Mn^{2+}]_{50}^{corr}$ (μM)	$^{E53Q}[Mn^{2+}]_{50}^{corr}$ (μM)	$^{E53Q}[Mn^{2+}]_{50}^{corr}/{}^{WT}[Mn^{2+}]_{50}^{corr}$	$(^{E53Q}[Mn^{2+}]_{50}^{corr}/{}^{WT}[Mn^{2+}]_{50}^{corr})^{1/6}$
Gly-37	NH	loop I	12.1	7.76	0.64	0.93
Glu-57	NH	helix I	8.96	26.4	2.95	1.20
Gly-38	NH	loop I	6.72	24.7	3.68	1.24
Val-58	NH	loop I	23.0	96.0	4.17	1.27
Lys-39	NH	helix I	3.60	15.5	4.31	1.28
Glu-56	NH	helix I	12.8	129	10.1	1.47
Glu-98	NH	loop III	11.3	121	10.7	1.48
Glu/Gln-53	NH	helix I	7.05	145	20.6	1.66

With the other mutants that were studied, complete displacement of the one tightly bound Mn^{2+} by Mg^{2+} was observed, as indicated by an ϵ^* value approaching unity and, independently, by EPR (data not shown). The dissociation constants of the binary E−Mg^{2+} complexes, $K_d^{Mg^{2+}}$ (Table 3), generally showed reasonable agreement with the corresponding activator constants of Mg^{2+} obtained kinetically, $K_a^{Mg^{2+}}$ (Table 1). With the E98D mutant, however, the $K_a^{Mg^{2+}}$ was 5.6-fold higher than the $K_d^{Mg^{2+}}$ (Tables 1 and 3).

The $K_d^{Mg^{2+}}$ values of the E56Q and E56D mutants were 2.1- and 1.4-fold greater than that of the wild type enzyme, respectively, while the $K_d^{Mg^{2+}}$ values of the E98Q and E98D mutants overlapped with that of the wild type enzyme (Tables 1 and 3), again indicating that Glu-56, but not Glu-98, contributes to metal binding in the binary E−Mg^{2+} complex. With the E44D mutant, the affinity for Mg^{2+} *increased* 2.4-fold compared to that of wild type enzyme, indicating an intact metal binding site.

^1H−^{15}N HSQC Titrations of the E53Q, E56Q, and E44D Mutants with $MgCl_2$. The locations and affinities of Mg^{2+} binding to three of the most kinetically damaged mutants were independently studied by direct Mg^{2+} titrations of ^{15}N-labeled proteins. With wild type MutT, the solution structure of the quaternary MutT−M^{2+}−AMPCPP−M^{2+} complex shows that the enzyme-bound divalent cation is coordinated by ligands Glu-56, -57, and -98 and the carbonyl group of Gly-38 (Figure 2) (*12*). Accordingly, the binding of Mg^{2+} to wild type MutT, when monitored by ^1H−^{15}N HSQC titrations, was previously shown to result in changes in chemical shifts of backbone NH resonances in loop III (residues 95−100), in helix I (residues 53−59), and to a lesser extent in loop I (*13*) all of which constitute the active site.

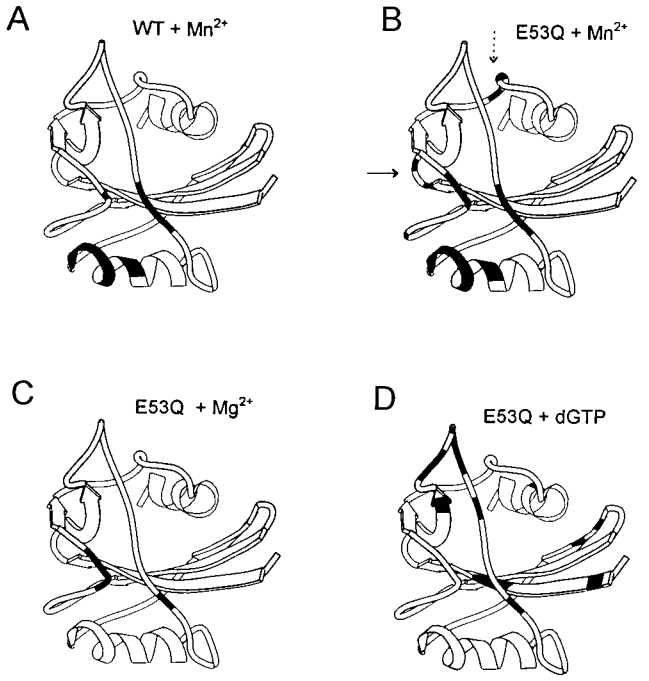

FIGURE 8: Regions of the E53Q mutant enzyme affected by metal or substrate binding. Sites of distance-dependent resonance disappearance in $^1H-^{15}N$ HSQC spectra induced (A) by Mn^{2+} (6 μM) binding to wild type and (B) by Mn^{2+} (60 μM) binding to the E53Q mutant of MutT. In panel B, the solid and dashed arrows indicate two additional Mn^{2+} binding sites in β-turn I and loop IV, respectively. Sites of ^{15}N and/or NH chemical shift changes in $^1H-^{15}N$ HSQC spectra of the E53Q mutant of MutT resulting from either (C) Mg^{2+} binding or (D) dGTP binding.

With the E53Q mutant, the changes in chemical shifts ($\Delta\delta$) of the ^{15}N and NH resonances produced by saturation with $MgCl_2$ (30 mM) are plotted according to residue number in panels A−C of Figure 9. In this titration, tracing the changes in chemical shifts of the amide resonances also permitted the assignment of the $^{15}N-^1H$ amide cross-peaks of all 115 of the non-proline residues of the E53Q mutant in the $E-Mg^{2+}$ complex. As summarized in Figure 8C, the effects of Mg^{2+} binding to the E53Q mutant were similar to those observed for the wild type enzyme, with the strongest effects being observed for residues 95−100 on loop III and to a lesser extent Lys-39 on loop I of the active site. However, in contrast to wild type MutT, no significant changes in chemical shifts were observed for residues 53−59 in helix I despite the fact that divalent cations bind in this region of the E53Q mutant as found by the strongest paramagnetic effects of Mn^{2+} (Figures 7A,B and 8B and Tables 4 and 5). Presumably, the E53Q mutation itself, by charge neutralization, had already produced chemical shift changes along the backbone of helix I (Figure 5A), and Mg^{2+} binding produced no further changes in this region. Similar behavior was observed with the metal-liganding mutant E57Q and its Mg^{2+} complex (*13*).

Using eq 3 and the $\Delta\delta(^{15}N)$ values for the backbone ^{15}N resonances of Lys-97, Gly-99, and Gln-100 and the side chain $^{15}N\epsilon$ resonance of Gln-53, a $K_d^{Mg^{2+}}$ of 15 ± 2 mM for the binding of Mg^{2+} to the E53Q mutant was determined (Figure 9D and Table 3). This value agrees well with the $K_d^{Mg^{2+}}$ of 21 ± 4 mM determined by displacement of Mn^{2+} from one of its three binding sites (Table 3), and establishes active site binding of Mg^{2+}. These values are significantly greater than the $K_d^{Mg^{2+}}$ of 1.4 ± 0.2 mM for wild type MutT as determined by HSQC titration (*13*) and by competition with Mn^{2+} ($K_d^{Mg^{2+}} = 7.5 \pm 1.2$ mM) (*10*) (Table 3), further indicating that Glu-53 interacts with the divalent cation in the binary complex.

Titration of the E56Q mutant with $MgCl_2$ produced small changes in chemical shifts of backbone NH signals of residues widely distributed around the metal binding site (data not shown), similar to those found with the E53Q (Figure 8C) and E57Q mutants (*13*). At the highest concentration of Mg^{2+} (28 mM), no significant changes in chemical shifts occurred along helix I, including those of the $^{15}N\epsilon$ resonance of Gln-56. The largest chemical shift change was that of the backbone ^{15}N of Glu-44, a conserved residue which precedes and stabilizes helix I. Using eq 3 and the $\Delta\delta(^{15}N$ or NH) values of this resonance and those of four other residues that exhibited sizable changes, namely, Val-8 (in β-strand A), Arg-22 (in β-strand B), Thr-81 (in β-strand D), and Gly-99 (in loop III), a $K_d^{Mg^{2+}}$ of 46 ± 18 mM for the binding of Mg^{2+} to the E56Q mutant at 32 °C was determined (Table 3). This value is comparable to the $K_a^{Mg^{2+}}$ (32 ± 4 mM, Table 1) and to the $K_d^{Mg^{2+}}$ determined by competition with Mn^{2+} (16 ± 2 mM, Table 3), both of which were measured at 23 °C, and is 33-fold higher than the $K_d^{Mg^{2+}}$ of the wild type enzyme (measured at 32 °C) (*13*), consistent with the loss of a metal ligand in the E56Q mutant. The order of magnitude greater weakening effect of the E56Q mutation on Mg^{2+} binding at 32 versus 23 °C (Table 3) suggests a significant enthalpic contribution to Mg^{2+} binding by Glu-56.

Titration of the E44D mutant with $MgCl_2$ produced sizable changes in chemical shifts in the loop I−helix I−loop II region, and also at Ala-7 (in β-strand A), Tyr-73 (in β-strand C), and Gln-100 (in loop III) (data not shown), similar to those previously observed with the wild type enzyme (*13*). The $K_d^{Mg^{2+}}$ of 1.5 ± 0.2 mM determined by these titrations agrees with that of the wild type enzyme (Table 3), further supporting an intact metal binding site in the E44D mutant.

$^1H-^{15}N$ HSQC Titrations of the E53Q, E56Q, and E44D Mutants with dGTP. To examine the intactness of the nucleotide-binding site, substrate titrations with dGTP were carried out. Previous titrations of wild type MutT with dGTP, monitored with $^1H-^{15}N$ HSQC spectra, yielded a dissociation constant for dGTP of 3.4 ± 0.3 mM (Table 3) and revealed changes in backbone ^{15}N and NH chemical shifts of residues on β-strands A−D, on loops I and IV, and at the beginning of helix II (*13*). The solution structure of the free MutT enzyme (*11*) shows that these regions form the walls of a cleft defined by the three β-strands (A, C, and D) on one side and loop I, the end of loop IV, and the beginning of helix II on the other side (Figure 1). The side chain $N\delta H_2$ group of Asn-119 at the beginning of helix II was found to interact favorably with the 6-keto group of the guanine base of dGTP as indicated by the downfield shift of one of the two $N\delta H_2$ resonances on dGTP binding and by the solution structure of the quaternary $MutT-M^{2+}-AMPCPP-M^{2+}$ complex (*12*, *13*).

$^1H-^{15}N$ HSQC titrations of the kinetically most damaged E53Q mutant were carried out with dGTP in the absence of divalent cations. Changes in chemical shifts ($\Delta\delta$) of the ^{15}N and NH resonances of the E53Q mutant at a saturating concentration of dGTP (7 mM) are plotted according to

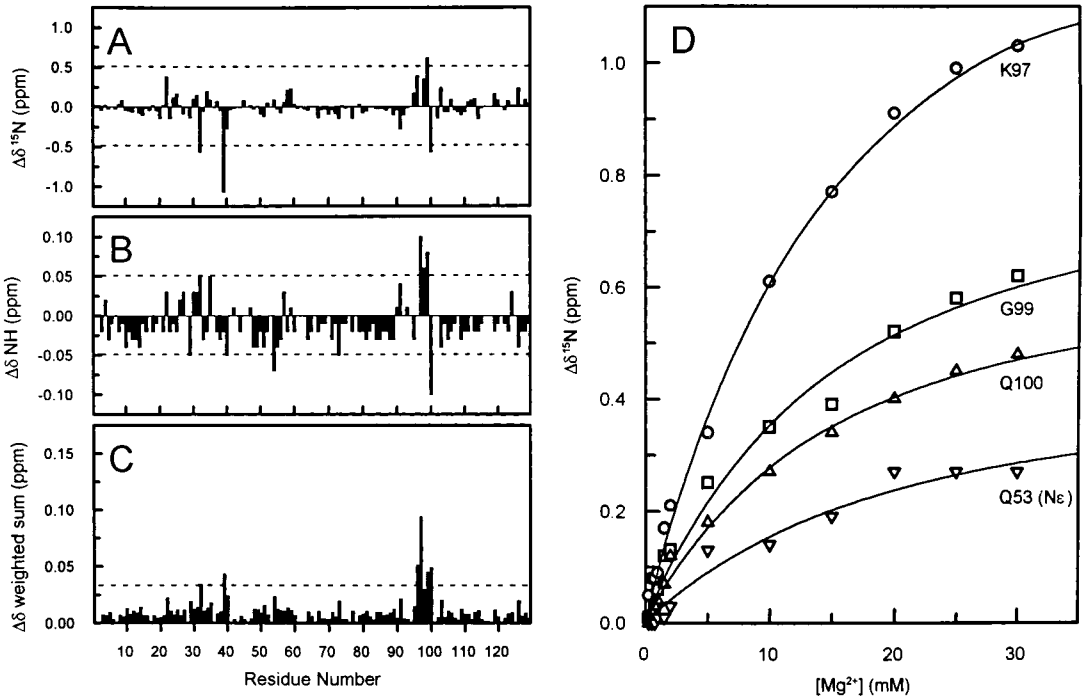

FIGURE 9: Changes in the backbone amide chemical shifts of the E53Q mutant upon binding of Mg^{2+} and determination of the dissociation constant for the E53Q−Mg^{2+} complex. Chemical shift changes ($\Delta\delta = \delta_{\text{free enzyme}} - \delta_{\text{complex}}$) were calculated on the basis of the chemical shift values obtained from ^{1}H−^{15}N HSQC spectra at 0 and 30 mM Mg^{2+} and plotted vs the residue number of wild type MutT. (A) ^{15}N chemical shift differences. (B) NH chemical shift differences. (C) Sum of the absolute magnitudes of the ^{15}N and NH chemical shift changes which were weighted according to the backbone amide chemical shift dispersion in the ^{15}N and ^{1}H dimensions (27.16 and 2.11 ppm, respectively) of the free E53Q mutant's spectra. The dashed lines indicate the error limits. (D) The amide nitrogen chemical shift changes of Lys-97 (○), Gly-99 (□), and Gln-100 (△) and the side chain ϵ-nitrogen chemical shift changes of Gln-53 (▽) were followed in ^{1}H−^{15}N HSQC spectra as the enzyme was titrated with Mg^{2+}. The curves are described by eq 3 using dissociation constants K_d of 14.4 ± 1.6 (○), 13.9 ± 2.9 (□), 13.7 ± 2.0 (△), and 19.6 ± 7.4 mM (▽) which yield a mean K_d value of 15.4 ± 2.4 mM for binding of Mg^{2+} to the E53Q mutant enzyme. From the dissociation constant for binding of Mg^{2+} to the E53Q mutant and eq 3, the occupancy is calculated to be 66% at the highest concentration of Mg^{2+} (30 mM) in the titration used for the final ^{15}N and NH $\Delta\delta$ values depicted in panels A−C.

residue number in Figure 10A−C. Tracing the changes in chemical shifts of the amide resonances during the titration permitted the assignment of the ^{15}N−^{1}H amide cross-peaks of all 115 of the non-proline residues of the E53Q mutant in the enzyme−dGTP complex. As summarized in Figures 10C and 8D, nucleotide binding to the E53Q mutant produced significant changes in ^{15}N and NH chemical shifts of residues on β-strands A−C, on loop I, and at the beginning of helix II at positions very similar to those observed with the wild type enzyme (*13*), consistent with an intact substrate binding site in the E53Q mutant. Using eq 3 and the $\Delta\delta$-(^{15}N) values of the backbone ^{15}N resonances of Val-8, Gly-9, and Glu-74 and the side chain ^{15}Nδ resonance of Asn-119, a K_d^{dGTP} of 0.48 ± 0.05 mM for the binding of dGTP to the E53Q mutant was determined (Figure 10D and Table 3). This 7-fold increase in affinity for dGTP, compared to that of wild type MutT, confirms an intact substrate binding site.

HSQC titrations of the E56Q and E44D mutants with dGTP resulted in significant chemical shift changes in many resonances, most of which are assigned to residues in the cleft region as found with wild type MutT (*13*), the E57Q mutant (*13*), and the E53Q mutant (Figure 8D). For the E56Q mutant, analysis of the titration curves of those residues which exhibited the largest chemical shift changes, namely, Val-8 and Gly-9 (in β-strand A), Ala-30, Lys-39, and Glu-44 (in loop I), Glu-74 (in β-strand D), and Asn-119 (in helix II), by fitting them to eq 3, yielded a K_d^{dGTP} of 0.97 ± 0.42 mM for the E56Q−dGTP complex at 32 °C (Table 3). This value is 3.5-fold tighter than that of the wild type enzyme, indicating an intact substrate binding site. For the E44D mutant, analysis of the titration curves of the shifted resonances of Val-8, Thr-21, Ile-80, and Asn-119 yielded a K_d^{dGTP} of 0.60 ± 0.20 mM. The errors in this dissociation constant are large because of smaller changes in the $\Delta\delta$ values. Nonetheless, this value is ∼6-fold tighter than that of the wild type enzyme (Table 3), again indicating an intact substrate binding site.

The reasons for the increased affinities for dGTP in the E53Q, E56Q, and E44D mutants are not clear. They are probably not due to the loss of negative charge because tightening of nucleotide binding is seen with the E44D mutant (Table 3), and is also detected kinetically with the E53D, E56D, and E44D mutants by the decreases in $K_s^{dGTP-Mg^{2+}}$ (Table 1).

Proposed Mechanism of the MutT Pyrophosphohydrolase. The conserved residue, Glu-53, is found to contribute $10^{4.7}$-fold to catalysis by the MutT pyrophosphohydrolase as suggested by the decrease in k_{cat} of the E53Q mutant. As determined by ^{1}H−^{15}N HSQC and ^{15}N-edited NOESY spectra, the structure of the most kinetically damaged E53Q mutant is largely intact with only small changes near the site of mutation.

Several observations indicate that Glu-53 functions as a direct ligand to the enzyme-bound divalent cation activator in the binary E−M^{2+} complex (Figure 11A). An order of magnitude weaker binding of Mn^{2+} to the E53D and E53Q mutants is detected by EPR (Table 3) and, in the case of

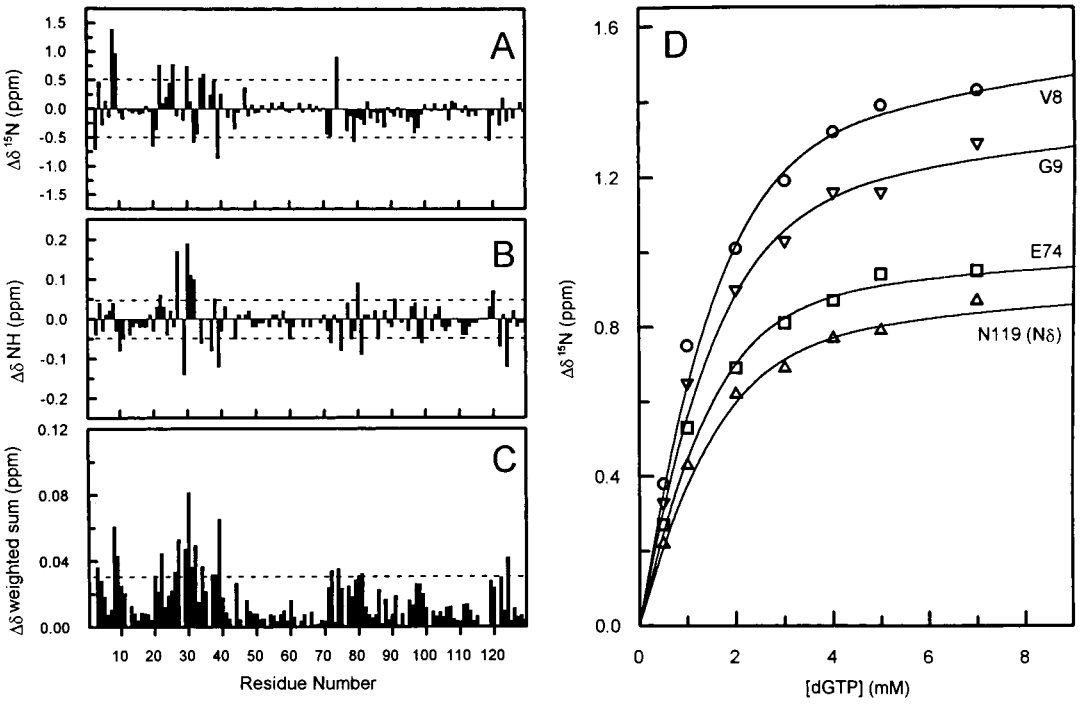

FIGURE 10: Changes in the backbone amide chemical shifts of the E53Q mutant upon binding of dGTP and determination of the dissociation constant of the E53Q−dGTP complex. Chemical shift changes ($\Delta\delta = \delta_{\text{free enzyme}} - \delta_{\text{complex}}$) were calculated on the basis of the chemical shift values obtained from $^1H-^{15}N$ HSQC spectra at 0 and 7 mM dGTP and plotted vs the residue number of wild type MutT. (A) ^{15}N chemical shift differences. (B) NH chemical shift differences. (C) Sum of the absolute magnitudes of the ^{15}N and NH chemical shift changes which were weighted according to the backbone amide chemical shift dispersion in the ^{15}N and ^1H dimensions (27.36 and 2.28 ppm, respectively) of the E53Q mutant enzyme's spectra. The dashed lines indicate the error limits. (D) The backbone amide ^{15}N chemical shift changes of Val-8 (○), Gly-9 (▽), and Glu-74 (□) and the side chain $^{15}N\delta$ chemical shift changes of Asn-119 (△) were followed in $^1H-^{15}N$ HSQC spectra as the enzyme was titrated with dGTP, and the curves are described by eq 3 using dissociation constants K_d of 0.50 ± 0.10 (○), 0.39 ± 0.11 (▽), 0.51 ± 0.11 (□), and 0.51 ± 0.12 mM (△) which yield a mean K_d value of 0.48 ± 0.05 mM for binding of dGTP to the E53Q mutant enzyme. From the dissociation constant for binding of dGTP to the E53Q mutant and eq 3, the occupancy is calculated to be 93% at the highest concentration of dGTP (7 mM) in the titration used for the final ^{15}N and NH $\Delta\delta$ values depicted in panels A−C.

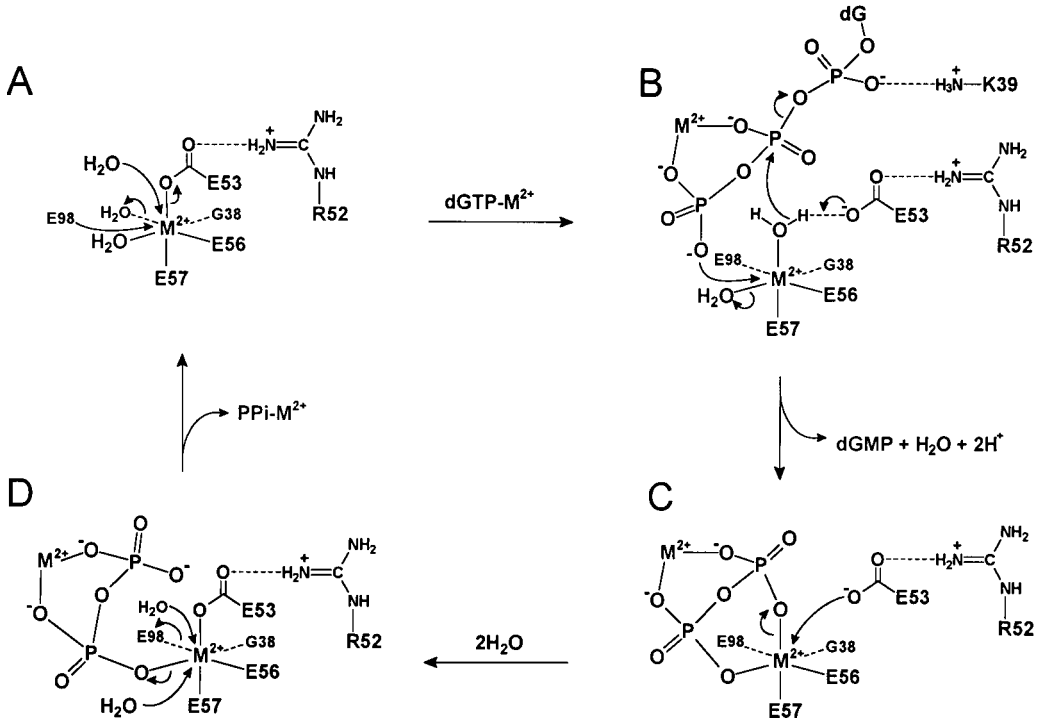

FIGURE 11: Proposed mechanism of the MutT reaction consistent with the solution structure of the quaternary MutT−M^{2+}−AMPCPP−M^{2+} complex (*12*), kinetic and mutagenesis studies (*10*, *12*−*14*; Table 1), and binding studies (Table 3).

E53D, by kinetic analysis (Table 1). Comparable weakening of Mg^{2+} binding by the E53D and E53Q mutants is found by titrations in competition with Mn^{2+} and by direct $^1H-^{15}N$ HSQC titration of the E53Q mutant (Table 3). A change

in the coordination sphere of enzyme-bound Mn^{2+} on both the E53Q and E53D mutants is indicated by a decrease in the enhanced paramagnetic effects of Mn^{2+} on $1/T_1$ of its water ligands. Direct Mn^{2+} titration of the E53Q mutant, by monitoring the paramagnetic broadening of assigned ^{15}N and NH resonances of the protein, shows Mn^{2+} to interact most closely with the NϵH$_2$ protons of Gln-53 (Table 4). Changes in the relative sensitivities of ^{15}N and NH resonances to broadening by Mn^{2+} in the E53Q mutant suggest that the enzyme-bound metal has moved (Tables 4 and 5) which may contribute to the decreased catalytic activity.

Water proton relaxation measurements suggest that in both the binary (Figure 11A) and quaternary complexes (Figure 11B), the enzyme-bound Mn^{2+} coordinates two water ligands (*10*, *12*). No significant decreases in the affinity of the E98Q and E98D mutants for Mn^{2+} or Mg^{2+} were detected in direct metal binding studies (Table 3), which does not support metal coordination by Glu-98 in the binary E$-M^{2+}$ complex, despite the proximity of this residue (*12*). Hence, to preserve the octahedral coordination of the enzyme-bound divalent cation in the binary complex, its ligands are reasonably assigned to Gly-38, Glu-53, -56, and -57, and two water molecules (Figure 11A), although other liganding arrangements cannot be ruled out. However, in the active quaternary complex, as indicated by 3−12-fold increases in K_m^{M2+} with the E98Q and E98D mutants (Table 1), significant weakening of metal binding is detected, suggesting direct metal coordination by Glu-98 (Figure 11B). In the quaternary complex, Glu-53 must dissociate from the metal to function as a general base to orient and deprotonate the attacking water ligand. To preserve octahedral coordination with two water ligands, Glu-98 is proposed to enter the coordination sphere of the enzyme-bound divalent cation in the quaternary complex (Figure 11B).

A role as a general base for Glu-53 is suggested by two observations. (i) The E53D mutation results in $10^{2.1}$-fold less damage to catalysis than that resulting from the E53Q mutation (Table 1), demonstrating the importance of an anionic residue at this position. (ii) The ascending limb from pH 6 to 8 of the pH dependence of k_{cat} of the wild type enzyme and the E53D mutant is not present in the pH dependence of k_{cat} of the E53Q mutant (Figure 3). The $10^{4.7}$-fold loss of activity in the E53Q mutant is consistent with other cases of loss of general base catalysis by mutagenesis (*38*). A metal-bound water ligand was proposed to be the attacking nucleophile because of its optimum positioning 4.2 Å from the β-phosphorus and 2.6 Å from the carboxylate oxygen of Glu-53 in the solution structure of the quaternary complex (*12*). Moreover, metal coordination would lower the pK_a of the attacking water, facilitating its deprotonation by Glu-53.

The attack on the β-phosphorus by the water ligand would create a monodentate β-phosphoryl complex of the enzyme-bound metal (Figure 11B). Such monodentate complexes readily form bidentate chelate rings with strong thermodynamic and kinetic driving forces (*39*, *40*). Hence, we suggest that the unfavorable nucleophilic displacement at the β-phosphorus may be driven in part by chelation of the enzyme-bound metal by both the β- and γ-phosphoryl groups of dGTP as well as by Lys-39 which facilitates the departure of the dGMP leaving group (Figure 11B → C). A recent X-ray structure of hypoxanthine phosphoribosyltransferase complexed with the primary substrate phosphoribosylpyrophosphate and an analogue of the substrate xanthine reveals two metal ions, each interacting with two pyrophosphate oxygens (*41*) similar to the proposed structure in Figure 11C. The final role for Glu-53 is to break the chelation of the enzyme-bound divalent cation by the PP_i-M^{2+} product (Figure 11C → D), permitting the facile displacement of PP_i-M^{2+} by water (Figure 11D → A). With wild type MutT, the pH dependence and viscogen independence of k_{cat} suggest that the attack step (Figure 11B → C) is rate-limiting, while with the severely kinetically damaged E53Q mutant, either the attack step or the chelation breakage step (Figure 11C → D) or both are rate-limiting.

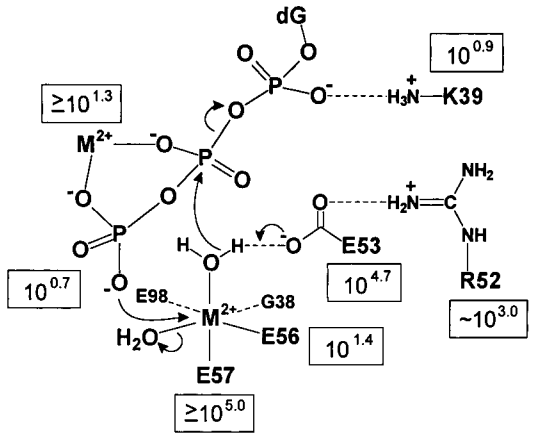

FIGURE 12: Contributions of active site residues to the overall catalytic power of the MutT pyrophosphohydrolase, as discussed in the text. Contributions are from the effects of mutations on k_{cat} in this paper (Table 1) and in refs *10* and *12*−*14*.

Multiple roles have also been proposed for the highly mobile residue, Glu-43, in staphylococcal nuclease which may serve as a ligand to Ca^{2+} in the binary E$-Ca^{2+}$ complex and as a general base in the active ternary E$-Ca^{2+}-$DNA complex (*42*). Similarly, Glu-172 of glyoxalase I serves as a metal ligand in the binary E$-Zn^{2+}$ complex and as a general base in the ternary E$-Zn^{2+}-$substrate complex (*43*). Also, on triosephosphate isomerase the mobile general base, Glu-165, deprotonates C-1 and reprotonates C-2 of the substrate (*44*), and on ketosteroid isomerase Asp-38, a mobile general base, deprotonates C-4 and reprotonates C-6 of the steroid (*45*). Thus, the mobility of general bases on enzymes may be essential to their optimum functioning in catalysis.

Contributions to the Catalytic Power of the MutT Enzyme. The active site mutants of the MutT enzyme studied here (Table 1) and in preceding papers (*10*, *12*−*14*) now permit us to evaluate the sources of the catalytic power of this enzyme. The Mg^{2+}-activated MutT enzyme, with a k_{cat} value of 4.0 s^{-1} (*10*), increases the rate of nucleophilic substitution at the electron-rich β-phosphorus of dGTP by a factor of $10^{9.0}$ when compared with the rates of model reactions extrapolated to the same temperature and pH (*3*). Figure 12 summarizes the contributions of active site residues to the overall catalytic power as indicated by the effects on k_{cat} of mutating these residues. A major contribution of at least 10^5-fold to the catalytic power is provided by the enzyme-bound divalent cation which polarizes and presents the attacking water or hydroxyl nucleophile to the β-phosphorus promoting catalysis by approximation. The factor of $\geq 10^5$ is suggested by the effects on k_{cat} of mutating the liganding residue Glu-

57, which is trans to the attacking water, to Gln, resulting in an altered position of the enzyme-bound divalent cation (*13*). Mutation of the cis-liganding residues Glu-56 and Glu-98 decreased k_{cat} by much smaller factors (Table 1), presumably due to a much smaller displacement of the metal ion. Apparently, these cis ligands fine-tune the position of the metal in the quaternary $E-M^{2+}-dGTP-M^{2+}$ complex and thereby the enzymatic activity. The 2-fold greater decrease in k_{cat} of the E56D mutation in comparison with the E56Q mutation indicates that ligand size at this position is more important to catalysis than ligand charge. Because all of the ligands to the enzyme-bound divalent cation contribute to its proper positioning, the smaller effects of the E56Q and E98Q mutations on k_{cat} are assumed to be contained in the $\geq 10^5$-fold effect of the E57Q mutation, and are not counted as separate contributions to the overall catalytic power.

Another major contribution of $10^{4.7}$ to catalysis is provided by Glu-53 which is proposed to orient and deprotonate the attacking water ligand in the chemical step and, in the next step, to facilitate the departure of the PP_i-M^{2+} product from the $E-M^{2+}-PP_i-M^{2+}$ complex, by displacing it from the enzyme-bound divalent cation. For these roles, charge is more important than size since the E53D mutant is $10^{2.1}$-fold more active than the E53Q mutant (Table 1). Since Arg-52 can contribute only indirectly to catalysis by orienting Glu-53 (*12*), its contribution is assumed to be contained in the $10^{4.7}$-fold effect of mutating Glu-53 to Gln, and is not counted separately.

Another factor of ~8 in catalytic power is provided by Lys-39 which electrostatically promotes the departure of the dGTP leaving group in the chemical step as suggested by the effect of the K39Q mutation on k_{cat} (*14*) and by the effect of pH on k_{cat} of wild type MutT and the K39Q mutant (Figure 3). The nucleotide-bound divalent cation contributes a factor of ≥ 20 to catalysis by charge neutralization at the β-phosphorus as suggested by the effect on activity of replacing Mg^{2+} at this position with Co^{3+} (*10*).

The conserved residue, Glu-44, while remote from the active site, is in the loop which immediately precedes helix I. Many of the liganding and catalytic residues are located in helix I (residues 47−59). Mutations of Glu-44 to Gln and especially to Asp profoundly decrease k_{cat} with Mg^{2+} as the activator but are less damaging to k_{cat} with Mn^{2+} as the activator (Table 1). Metal and substrate binding are unaffected or tightened by these mutations (Table 3), and structural changes in the kinetically more damaged E44D mutant are largely limited to the loop I−helix I motif. These observations suggest that Glu-44 influences the structure of loop I which, in turn, stabilizes helix I. Mutations of Glu-44 alter the structure of loop I, thereby destabilizing helix I in the transition state, decreasing k_{cat}. The metal activator Mn^{2+}, which binds more tightly to all forms of MutT than Mg^{2+} (Tables 1 and 3), apparently can reverse this destabilization more than Mg^{2+} can.

The product of the contributions to catalysis by the enzyme-bound divalent cation ($\geq 10^{5.0}$), the catalytic residues Glu-53 ($10^{4.7}$) and Lys-39 ($10^{0.9}$), and the nucleotide-bound divalent cation ($\geq 10^{1.3}$) exceeds $10^{11.9}$ which is at least $10^{2.9}$-fold greater than the catalytic power of the MutT enzyme ($10^{9.0}$). Hence, these contributions to catalysis (i.e., exponents) must be *partially* additive rather than additive (*46*). Partial additivity of the effects of mutations on k_{cat} has been shown theoretically and experimentally to result from cooperatively interacting residues facilitating the same step or, alternatively, from noninteracting residues facilitating consecutive non-rate-limiting steps (*46*). In the former case, the departure from additivity ($\geq 10^{2.9}$) provides a measure of the cooperativity. Since all four of these contributions occur, at least in part during the chemical steps, ample opportunity for cooperativity, and hence partial additivity, exists. As pointed out previously (*46*), such cooperative interactions may be investigated more directly by the effects on catalysis of double mutants.

ACKNOWLEDGMENT

We thank Dr. Stephen J. Gould for use of his PCR apparatus, Brian Geisbrecht and Dr. Suzanne O'Handley for advice on mutagenesis, and Dr. Maurice Bessman for providing the *E. coli* strain which overexpressed the K39Q mutant.

REFERENCES

1. Bhatnagar, S. K., Bullions, L. C., and Bessman, M. J. (1991) *J. Biol. Chem. 266*, 9050−9054.
2. Weber, D. J., Abeygunawardana, C., Bessman, M. J., and Mildvan, A. S. (1993) *Biochemistry 32*, 13081−13088.
3. Mildvan, A. S., Weber, D. J., and Abeygunawardana, C. (1999) *Adv. Enzymol. Relat. Areas Mol. Biol. 73*, 183−207.
4. Yanofsky, C., Cox, E. C., and Horn, V. (1966) *Proc. Natl. Acad. Sci. U.S.A. 55*, 274−281.
5. Maki, H., and Sekiguchi, M. (1992) *Nature 355*, 273−275.
6. Cheng, K. C., Cahill, D. S., Kasai, H., Nishimura, S., and Loeb, L. A. (1992) *J. Biol. Chem. 267*, 166−172.
7. Mo, J. Y., Maki, H., and Sekiguchi, M. (1992) *Proc. Natl. Acad. Sci. U.S.A. 89*, 11021−11025.
8. Sakumi, K., Furuichi, M., Tsuzuki, T., Kakuma, T., Kawabata, S., Maki, H., and Sekiguchi, M. (1993) *J. Biol. Chem. 268*, 23524−23530.
9. Kakuma, T., Nishida, J., Tsuzuki, T., and Sekiguchi, M. (1995) *J. Biol. Chem. 270*, 25942−25948.
10. Frick, D. N., Weber, D. J., Gillespie, J. R., Bessman, M. J., and Mildvan, A. S. (1994) *J. Biol. Chem. 269*, 1794−1803.
11. Abeygunawardana, C., Weber, D. J., Gittis, A. G., Frick, D. N., Lin, J., Miller, A.-F., Bessman, M. J., and Mildvan, A. S. (1995) *Biochemistry 34*, 14997−15005.
12. Lin, J., Abeygunawardana, C., Frick, D. N., Bessman, M. J., and Mildvan, A. S. (1997) *Biochemistry 36*, 1199−1211.
13. Lin, J., Abeygunawardana, C., Frick, D. N., Bessman, M. J., and Mildvan, A. S. (1996) *Biochemistry 35*, 6715−6726.
14. Frick, D. N., Weber, D. J., Abeygunawardana, C., Gittis, A. G., Bessman, M. J., and Mildvan, A. S. (1995) *Biochemistry 34*, 5577−5586.
15. Harris, T. K., Wu, G., and Mildvan, A. S. (1999) *FASEB J. 13*, A1353.
16. Wu, G., Harris, T. K., and Mildvan, A. S. (1999) *FASEB J. 13*, A1353.
17. Abeygunawardana, C., Weber, D. J., Frick, D. N., Bessman, M. J., and Mildvan, A. S. (1993) *Biochemistry 32*, 13071−13080.
18. Sambrook, J., Fritsch, E. F., and Maniatis, T. (1989) in *Molecular Cloning*, Cold Spring Harbor Laboratory Press, Plainview, NY.
19. Sarkar, G., and Sommer, S. S. (1990) *BioTechniques 8*, 404−407.
20. Barik, S. (1993) in *PCR Protocol: Current Methods and Applications* (White, B. A., Ed.) Vol. 15, pp 277−286, Humana Press, Inc., Totowa, NJ.
21. Barnes, W. M. (1994) *Proc. Natl. Acad. Sci. U.S.A. 91*, 2216−2220.
22. Cohn, M., and Townsend, J. (1954) *Nature 173*, 1090−1091.
23. Mildvan, A. S., and Engle, J. L. (1972) *Methods Enzymol. 26C*, 654−682.

24. Piotto, M., Saudek, V., and Sklenar, V. (1992) *J. Biomol. NMR 2*, 661−665.
25. Marion, D., Driscoll, P. C., Kay, L. E., Wingfield, P. T., Bax, A., Gronenborn, A. M., and Clore, G. M. (1989) *Biochemistry 28*, 6150−6156.
26. Kay, L. E., Keifer, P., and Saarinen, T. (1992) *J. Am. Chem. Soc. 114*, 10663−10665.
27. Levy, G. C., and Lichter, R. L. (1979) in *Nitrogen-15 NMR Spectroscopy*, John Wiley & Sons, New York.
28. Zhang, O., Kay, L. E., Olivier, J. P., and Foreman-Kay, J. D. (1994) *J. Biomol. NMR 4*, 845−858.
29. Kay, L. E. (1993) *J. Am. Chem. Soc. 115*, 2055−2057.
30. Johnson, B. A., and Blevins, R. A. (1994) *J. Biomol. NMR 4*, 603.
31. Dawson, R. M. C., Elliot, D. C., Elliot, W. H., and Jones, K. M. (1986) in *Data for Biochemical Research*, pp 413−415, Oxford University Press, New York.
32. Segel, I. H. (1977) in *Enzyme Kinetics*, pp 884−924, John Wiley & Sons, New York.
33. Mildvan, A. S., and Gupta, R. K. (1978) *Methods Enzymol. 49G*, 322−359.
34. Serpersu, E. H., Shortle, D., and Mildvan, A. S. (1986) *Biochemistry 25*, 68−77.
35. Serpersu, E. H., Shortle, D., and Mildvan, A. S. (1987) *Biochemistry 26*, 1289−1300.
36. Zhao, Q., Abeygunawardana, C., and Mildvan, A. S. (1997) *Biochemistry 36*, 3458−3472.
37. Villafranca, J. J., and Mildvan, A. S. (1972) *J. Biol. Chem. 247*, 3454−3463.
38. Mildvan, A. S. (1997) *Proteins: Struct., Funct., Genet. 29*, 401−416.
39. Cotton, F. A., and Wilkinson, G. (1980) in *Advanced Inorganic Chemistry*, pp 71−74, John Wiley & Sons, New York.
40. Basolo, F., and Pearson, R. G. (1967) in *Mechanisms of Inorganic Reactions*, pp 223−228, John Wiley & Sons, New York.
41. Focia, P. J., Craig, S. P., III, and Eakin, A. E. (1998) *Biochemistry 37*, 17120−17127.
42. Serpersu, E. H., McCracken, J., Peisach, J., and Mildvan, A. S. (1988) *Biochemistry 27*, 8034−8044.
43. Cameron, A. D., Ridderström, M., Olin, B., Kavarana, M. J., Creighton, D. J., and Mannervik, B. (1999) *Biochemistry 38*, 13480−13490.
44. Harris, T. K., Cole, R. N., Comer, F. I., and Mildvan, A. S. (1998) *Biochemistry 37*, 16828−16838.
45. Kuliopulos, A., Mildvan, A. S., Shortle, D., and Talalay, P. (1989) *Biochemistry 28*, 149−159.
46. Mildvan, A. S., Weber, D. J., and Kuliopulos, A. (1992) *Arch. Biochem. Biophys. 294*, 327−340.

BI9918745